 doi:10.20944/preprints202203.0143.v1

Article

Physiological oxygen causes the release of volatile organic compounds from human pluripotent stem cells with possible roles in maintaining self-renewal and pluripotency

Sara Barreto [1,†], Mohammed A. Al-Zubaidi [1,2,†], Tina P. Dale [1], Amy J. Worrall [1], Zoher Kapacee [3], Susan J. Kimber [3], Josep Sulé-Suso [1,4], Nicholas R. Forsyth [1,*] and Abigail V. Rutter [1,*]

[1] School of Pharmacy and Bioengineering, Keele University, Stoke-on-Trent, Staffordshire, UK; s.barreto-francisco@keele.ac.uk (S.B.); m.al_zubaidi@uomustansiriyah.edu.iq (M.A.A.-Z.); t.p.dale@keele.ac.uk (T.P.D.); a.j.worrall1@keele.ac.uk (A.J.W.); zoher.kapacee@manchester.ac.uk (Z.K.); sue.kimber@manchester.ac.uk (S.J.K.); josep.sule-suso@uhnm.nhs.uk (J.S.-S.); n.r.forsyth@keele.ac.uk (N.R.F.); a.v.rutter@keele.ac.uk (A.V.R.)
[2] Department of Clinical Laboratory Sciences, College of Pharmacy, Mustansiriyah University, Baghdad, Iraq
[3] Division of Cell Matrix Biology and Regenerative Medicine, School of Biological Sciences, University of Manchester, Oxford Rd, Manchester M13 9PT
[4] Cancer Centre, University Hospital of North Midlands, Newcastle Road, Stoke-on-Trent, Staffordshire, UK
* Correspondence: a.v.rutter@keele.ac.uk; n.r.forsyth@keele.ac.uk
† Co-first author, these authors contributed equally to this work

Abstract:

Human pluripotent stem cells (hPSCs) have widespread potential biomedical applications. There is a need for large-scale *in vitro* production of hPSCs, and optimal culture methods are vital in achieving this. Physiological oxygen (2% O_2) improves key hPSCs attributes, including genomic integrity, viability, and clonogenicity, however, its impact on hPSC metabolism remains unclear. Here, Selected Ion Flow Tube-Mass Spectrometry (SIFT-MS) was used to detect and quantify metabolic Volatile Organic Compounds (VOCs) in the headspace of hPSCs and their differentiated progeny. hPSCs were cultured in either 2% O_2 or 21% O_2. Media was collected from cell cultures and transferred into glass bottles for SIFT-MS measurement. The VOCs acetaldehyde and dimethyl sulfide (DMS)/ethanethiol were significantly increased in undifferentiated hPSCs compared to their differentiating counterparts, and these observations were more apparent in 2% O_2. Pluripotent marker expression was consistent across both O_2 concentrations tested. Transcript levels of ADH4, ADH5, and CYP2E1, encoding enzymes involved in converting ethanol to acetaldehyde, were upregulated in 2% O_2, and chemical inhibition of ADH and CYP2E1 decreased acetaldehyde levels in hPSCs. Acetaldehyde and DMS/ethanethiol may be indicators of altered metabolism pathways in physiological oxygen culture conditions. The identification of non-destructive biomarkers for hPSC characterization has the potential to facilitate large-scale in vitro manufacture for future biomedical application.

Keywords: human pluripotent stem cells; human embryonic stem cells; human induced pluripotent stem cells; cellular metabolism; oxygen; self-renewal; pluripotency; differentiation; volatile organic compounds; Selected ion flow tube-mass spectrometry

1. Introduction

Human pluripotent stem cells (hPSCs), including human Embryonic Stem cells (hESCs) and human induced Pluripotent Stem Cells (hiPSCs), are capable of multiplying indefinitely and differentiating into cell types representative of the three germ layers [1]. These properties make hPSCs applicable across advancing biomedical fields including

Preprints (www.preprints.org) | NOT PEER-REVIEWED | Posted: 10 March 2022 doi:10.20944/preprints202203.0143.v1

regenerative medicine, disease modelling and drug discovery [1,2]. Large-scale *in vitro* production of hPSCs is required to exploit their full potential with downstream applications, including therapeutic application, demanding a significant number of cells [2–4]. Long-term culture of hPSCs is frequently associated with both spontaneous differentiation and the appearance of chromosomal abnormalities, increasing the risk of tumorigenesis and consequently hampering the further use of the cells [5–8]. Developing optimal *in vitro* culture conditions for expanding hPSCs can minimize cellular changes and improve cell safety for clinical applications [9–11].

While the majority of laboratories perform routine culture of hPSCs under hyperoxic, non-physiological, air oxygen (~21% O_2), this is higher than the O_2 level in the *in vivo* physiological microenvironment of the pre-implantation blastocyst (embryonic structure from where hESCs derived) (~1–5% O_2) [5,8,12,13]. This non-physiological O_2 results in oxidative stress, DNA damage, and genomic instability in hPSCs [5,8,9,13–16]. The precise impact of physoxia on hPSC culture will vary according to culture conditions being used, including culture media, substrate, passaging intervals and methods, and hPSC cell line [2]. Consistency in approach will aid in improving overall interpretation. Reported discrepancy between studies could result from the use of hPSC characterization assays that focus on assessing colony morphology, proliferation, pluripotency, differentiation capacity and genome integrity [17–19]. Cellular metabolism is rarely evaluated in these assays, and changes in hPSC self-renewal and pluripotency do not necessarily reflect changes in their metabolism [17,19]. Therefore, the effects of O_2 conditions on hPSC metabolism remain largely unknown. Analysis of the metabolic state of hPSCs under different O_2 conditions could provide detailed understanding of the impact of the surrounding environment on hPSC behaviors.

Cellular metabolism comprises all the biochemical reactions and their intermediates (i.e., metabolites) in a cell that are used to produce energy and components (building blocks, signaling molecules and redox reagents) indispensable for cell survival [20–23]. High proliferating cells, such as hPSCs, have specific energetic requirements to support growth and the production of new cells [23,24]. hPSCs rely primarily on glycolysis (conversion of glucose to lactate) to generate energy rather than oxidative phosphorylation even in the presence of oxygen (called the Warburg effect) [23,25,26]. Although glycolysis is less energetically efficient compared to oxidative phosphorylation (generation of 4 adenosine triphosphate (ATP) compared to 36 ATP, respectively), it can produce equal amounts (or more) of energy if there is sufficient glucose flux, i.e., in cell culture [25,26]. Most importantly, the metabolic intermediates of glycolysis, e.g., carbon, ribose and nicotinamide adenine dinucleotide phosphate (NADPH), are used in the production of nucleic acids, amino acids, lipids, and carbohydrates, essential for high proliferative growth [22,23,25,26]. Furthermore, the preference of glycolysis over oxidative phosphorylation reduces the risk of DNA damage caused by the formation of reactive oxygen species (ROS) associated with oxidative phosphorylation [26]. Although it is evident that hPSCs favor glycolysis for energy generation, mitochondrial metabolism is also utilized by the cells and influences their functions and fate [25]. For instance, hPSCs use the metabolic intermediates of mitochondrial tricarboxylic acid (TCA) cycle to serve as building blocks for many biosynthetic processes needed for cell division [25].

The metabolic activity of a cell can be described by the concentrations of metabolites and rates (or fluxes) at which a metabolite is produced or consumed [21]. Therefore, metabolites can be used as candidate biomarkers for describing a particular hPSC cellular state and reveal metabolic pathways that participate in specific hPSC functions [27]. Volatile organic compounds (VOCs) are metabolic products of the exometabolome (metabolites in the extracellular environment) that carry information of the metabolic activities occurring between cells and their environment [28,29]. They can be carboxylic acids, aldehydes, alcohols, alkanes, esters or ketones, and can represent a fingerprint of cell status as their emission patterns vary in response to changes in environmental conditions [30,31].

Preprints (www.preprints.org) | NOT PEER-REVIEWED | Posted: 10 March 2022 doi:10.20944/preprints202203.0143.v1

VOC analysis can be used for the study of cellular metabolism, and being non-invasive enables monitoring of metabolic changes over time [29].

VOCs and other metabolites can be identified using various metabolomics techniques, such as mass spectrometry and nuclear magnetic resonance based methods [32,33]. Various VOCs have already been identified in PSCs [34,35]. For example, mouse ESCs have been shown to release high concentrations of thiirane and methyl-methoxy-hydroxymethyl-amine after 72 hours in culture compared to fibroblasts. The identified VOCs had roles in extracellular matrix modulation [34], that participated in the maintenance of PSC functions [36]. Further, hiPSCs demonstrated significant differences in relative abundance of decanal, butanoic acid, 2-methylpropyl ester, propanoic acid, 2-methyl-, anhydride, 3-Hexanone, 2,4-dimethyl and 3,5-Dimethyl-4-octanone when compared to early neural progenitors [35]. Styrene and 1-hexanol-2-ethyl discriminated between hiPSCs and differentiating embryoid bodies.

Analytical platforms used to measure metabolites are generally invasive, lack sensitivity, and require complicated sample preparation [32]. Selected-ion flow-tube mass spectrometry (SIFT-MS) is an analytical technique that can overcome some of these issues. SIFT-MS is a non-invasive quantitative technique that detects VOCs in real-time [37,38]. It employs selected precursor ions that react during a defined reaction time with the gases present in the sample [37,38]. The product ions resulting from the ionization reactions are then used to identify the various molecules in the sample's headspace [39]. SIFT-MS has been widely used in breath and lung cancer research [39,40]. However, it has potential for application in fields, such as hPSC metabolomics, where the analysis of VOCs can provide mechanistic insights [40].

This study aimed to identify and quantify VOCs in the headspace of hPSCs and their differentiated progeny under physoxia (2% O_2) and air oxygen (21% O_2) using SIFT-MS. We detected differences in undifferentiated hPSCs and their differentiating counterparts cultured in the two distinct O_2 conditions. In contrast, standard approaches including proliferation and protein expression, detected no significant changes in the cells. VOCs were detected at differing concentrations in different hPSC lines and VOC profiles were distinct when cells were cultured in either 2% or 21% O_2. Undifferentiated hPSCs showed higher concentrations of the VOCs acetaldehyde and dimethyl sulfide (DMS)/ethanethiol compared to their progeny. Gene expression analysis also showed that 2% O_2 upregulated genes (ADH4, ADH5, and CYP2E1) encoding enzymes involved in converting ethanol into acetaldehyde, and downregulated genes (ALDH1A1, ALDH1A3, and ALDH6A1) encoding enzymes responsible for generating acetate from acetaldehyde in undifferentiated hPSCs. Chemical inhibition of the upregulated enzymes alcohol dehydrogenase (ADH) and cytochrome P450 2E1 (CYP2E1) in undifferentiated hPSCs resulted in increased ethanol in 2% O_2 and reduced acetaldehyde levels in both O_2 conditions, significantly so in 21%.

2. Materials and Methods

2.1. Human Pluripotent Stem Cell culture

hESC lines SHEF-1 and -2 (UK Stem Cells Bank) [41] and the hiPSC line ZK2012L (kindly provided by Prof. Susan J. Kimber, Faculty of Biology Medicine and Health, University of Manchester) were used in this study. The hiPSC ZK2012L line was generated from the reprogramming of human dermal fibroblasts by lentiviral transduction of the markers OCT4, SOX2, KLF4 and c-Myc [42].

hPSCs were routinely cultured using Essential 8 (E8) Medium (Gibco, Cat. No. A15169-01) in 6-well tissue culture plates coated with 0.5 μg/cm^2 truncated recombinant human vitronectin (rh VTN-N) (ThermoFisher Scientific, Cat. No. A14700) and maintained in a humidified incubator at 37 ^{o}C in the presence of 5% CO_2 and either 2% or 21% O_2. The medium was renewed daily until cells reached about 85% confluency after 4-5 days. hPSCs were then exposed to 0.5 mM UltraPure™ ethylene diamine tetra acetic acid

Preprints (www.preprints.org) | NOT PEER-REVIEWED | Posted: 10 March 2022 doi:10.20944/preprints202203.0143.v1

(EDTA) (Invitrogen, Cat. No. 15575020) in Dulbecco's phosphate buffer saline (DPBS) without calcium and magnesium (Gibco, Cat. No. 14190094) before being passaged as small clumps. Cells were observed daily under phase contrast (Nikon Eclipse TS100, Japan) to ensure maintenance of an undifferentiated morphology and to evaluate confluency levels.

2.2. Cell proliferation, viability and metabolic assays

Proliferation and viability of hPSCs was determined via standard hemocytometer cell counting with trypan blue (Sigma-Aldrich, Cat. No. T8154) exclusion. For this, hPSCs were passaged as single-cell suspensions using 1% Trypsin-Versene (EDTA) solution (Lonza, Cat. No. BE02-007E) in DPBS. Cells were mixed with trypan blue at 1:1 and counted under an inverted light microscope.

hPSC metabolic activity was evaluated using MTT (3-(4,5-dimethylthiazol-2-yl)-2,5-diphenyltetrazolium bromide) assay. Cells were seeded, 10,000 cells/well, and cultured in standard 96-well plates, at either 2% O_2 or 21% O_2, for 2 days. On days 3 to 7, individual wells were incubated with 0.5 mg/mL MTT reagent (Sigma-Aldrich, Cat. No. M5655) in E8 medium for 4 hours at 37 ^oC. Following this, 50 µl of dimethyl sulfoxide (DMSO) was added to each well and incubated for a further 45 minutes at 37 ^oC while protected from light. Absorbance at 570 nm was measured using a microplate reader (BioTek, Synergy 2). Three independent experiments were performed for both 2% O_2 and 21% O_2.

2.3. Live staining of hPSCs

Live staining of pluripotency-associated surface markers was performed using the GloLIVE™ Human Pluripotent Stem Cell Live Cell Imaging Kit (R&D Systems, Cat. No SC023) following the manufacturer's procedure. Briefly, 3.3 x 10^5 hPSCs were seeded into each well of a VTN-coated 6-well plate. After 4 days, media was replaced with 1 mL E8 containing 1X fluorochrome-conjugated antibody (SSEA-4, TRA-1-60(R), or SSEA-1) and incubated for 30 minutes at 37 ^oC. After incubation, media was removed, and hPSCs rinsed with E8 to eliminate any residual antibody, followed by addition of fresh E8 medium. Imaging of labelled hPSCs was carried out using a Nikon Eclipse Ti-S (Japan) fluorescence microscope equipped with a Nikon DS-Qi1Mc (Japan) camera. Image acquisition was performed using NIS-elements software (Nikon).

2.4. Flow Cytometry

hPSCs were enzymatically disaggregated into single cell suspension with Trypsin-Versene (EDTA) solution after which, 5 x 10^5 cells/well were seeded into 6-well plates and cultured for 4 days. Labelling was performed as described above (see section 2.3.). After removing the antibody-containing medium, hPSCs were washed with DPBS and dissociated with Trypsin-Versene (EDTA). Cell suspensions were centrifuged at 300 x g for 3 minutes. Supernatants removed, and cell pellets re-suspended in flow cytometer buffer [0.5% (w/v) Bovine Serum Albumin (BSA) (Fisher BioReagents, Cat. No. BP9703-100) and 2 mM EDTA in DPBS]. Samples were centrifuged once more, and pellets re-suspended in DPBS before analysis. Data acquisition was performed with a Cytomics FC 500 (Beckman Coulter) flow cytometer, and analysis completed using Flowing Software (version 2.5.1).

2.5. Spontaneous differentiation

Spontaneous differentiation of hPSCs was performed as previously described [43]. Approximately 5 x 10^5 hPSCs/well were seeded onto 6-well plates in both 2% and 21% O_2 conditions. After 2 days, E8 medium was replaced with spontaneous differentiation media (SDM), which consisted of Knockout Dulbecco's Modified Eagle Medium (KO-DMEM) (Gibco, Cat. No. 10829018) supplemented with 10% (v/v) Fetal Bovine Serum (FBS), 2 mM L-Glutamine (Lonza, Cat. No. BE17-605E), 1% (v/v) Minimum Essential Medium Non-Essential Amino Acid Solution (MEM-NEAA) (Lonza, Cat. No. BE13-114E)

Preprints (www.preprints.org) | NOT PEER-REVIEWED | Posted: 10 March 2022 doi:10.20944/preprints202203.0143.v1

and 0.1 mM 2-mercaptoethanol (Gibco, Cat. No. 31350010). Cells were cultured in SDM for 21 days with media changed every 3 days.

2.6. Immunocytochemistry

Pluripotent marker expression analysis was performed during differentiation (days 0, 5, 10 and 20). hPSCs were washed in DPBS, fixed with 4% paraformaldehyde (PFA) in DPBS for 30 minutes at room temperature, and washed 3 times with 1% BSA (Sigma-Aldrich, Cat. No. A1595) in DPBS. Fixed cells were permeabilized and blocked using 10% donkey serum (Sigma-Aldrich, Cat. No. D9663), 0.3% Triton X-100 (Sigma-Aldrich, Cat. No. T8787) and 1% BSA in DPBS, for 45 minutes at room temperature. Subsequently, hPSCs were incubated with 1 µg/100 µl of either mouse anti-alkaline phosphatase, mouse anti-SSEA-4, goat anti-Nanog, or goat anti-Oct 3/4 (R&D Systems, Cat. No. SC008) overnight at 2–8 °C followed by a repeated washes with 1% BSA before incubation with 5 µg/mL of appropriate secondary antibody for 1 hour at room temperature. Alkaline phosphatase and SSEA-4 were visualized with donkey anti-mouse IgG NL557 (R&D Biosystems, Cat No. NL007), and Nanog and Oct 3/4 were visualized with donkey anti-goat IgG NL493 (R&D Systems, Cat. No. NL003). Counterstaining was with DAPI (Sigma-Aldrich, Cat. No. D9542) at 100 ng/mL. Image acquisition was performed Nikon Eclipse Ti-S fluorescence microscope equipped with a Nikon DS-Qi1Mc camera and processed using NIS-elements software.

2.7. Reverse Transcriptase-Polymerase Chain Reaction (RT-PCR)

Gene expression analysis was performed at matched time points with immunocytochemistry. Cells were lysed, homogenized, and their RNA extracted using RNeasy Mini Kit (Qiagen, Cat. No. 74104) following the manufacturer's protocols. RNA concentration was measured using a Nanodrop 2000 spectrometer (Thermo Scientific, UK). One-step RT-PCR was performed using QIAGEN OneStep RT-PCR Kit (Cat. No. 210210) according to the manufacturer's instructions. Forward and reverse primers were designed using NCBI Primer-BLAST (see Table 1 for primers sequences and the corresponding annealing temperatures for each primer pair). All RT-PCR reactions consisted of one cycle of 50 °C for 30 minutes, one cycle of 95 °C for 15 minutes, followed by 39 repeated cycles of: 94 °C for 1 minute, primer specific annealing temperature (Table S1) for 1 minute, and 72 °C for 1 minute, this was followed by a final cycle of 72 °C for 10 minutes. Confirmation of the resulting PCR product amplification was accomplished through standard 2% agarose gel electrophoresis.

2.8. ADH and CYP2E1 inhibition

Inhibition of ADH and CYP2E1 was performed using 4-methyl pyrazole (4-MP) (Alfa Aesar, Cat. No. A18083). hPSCs were cultured to 70-80% confluency before 4-MP was added to fresh E8 media at 0.5 mM, 5 mM and 50 mM with incubation on cells for a further 72 hours. After incubation, MTT assay was performed to assess the viability of the hPSCs post-treatment (see section 2.2. for details of the procedure).

2.9. Selected Ion Flow Tube-Mass Spectrometry (SIFT-MS) measurement

The SIFT-MS technique has been described previously in detail [37]. hPSCs were cultured to 70-80% confluence before proceeding to SIFT-MS analysis (Figure 1). hPSCs were incubated in E8 medium (20 mL distributed in a 6-well plate) for 24 hours at 2% and 21% O_2. With hPSC differentiation, 20mL of fresh SDM was added to hPSCs at 4 different time points of differentiation (days 5, 10 and 20), and left to incubate for 24 hours on cells before removal for SIFT-MS. "Cell-free" media controls consisting of either E8 or SDM in 6-well plates were incubated for the same amount of time at the two O_2 conditions. Following incubation, both cell and cell-free media samples were transferred into sterile 150 mL glass bottles (Camlab, Cat. No. G801/05), covered with an aluminum screw cap and a black

 doi:10.20944/preprints202203.0143.v1

rubber septum. Additional "fresh media" controls composed of 20 mL of fresh E8 or SDM were transferred into two other glass bottles. 130 mL of bottle headspace was purged with dry compressed air (composed of 20% oxygen and 80% nitrogen, BOC, UK) for approximately 1 minute. Bottles were capped tightly to prevent air exchange between the bottle and the environment and transferred to a 37 °C and 5% CO_2 incubator. After 16 hours, each bottle was transferred to a 37 °C water bath for SIFT-MS measurement. The headspace of each sample was measured with Profile 3 SIFT-MS (Instrument Science, UK) via a hypodermic needle puncturing the septum of the cap, allowing the sample headspace to flow directly into the SIFT-MS instrument via a heated PEEK capillary line. 30 mL of sample headspace was analyzed for full scan mode (FSM) and multiple ion monitoring (MIM) mode using the H_3O^+ precursor ion. The sample measurement time was around 1 minute in total.

The same procedure was performed to measure the effects of ADH and CYP2E1 inhibition on the VOC profile of hPSCs cultured at 2% and 21% O_2. Non-treated and treated experimental groups were created for each hPSC line and each O_2 condition. Cells in the treated group were exposed to 5 mM 4-MP inhibitor for 24 hours. The corresponding cell-free media controls consisted of E8 with or without 5 mM 4-MP.

Preprints (www.preprints.org) | NOT PEER-REVIEWED | Posted: 10 March 2022 doi:10.20944/preprints202203.0143.v1

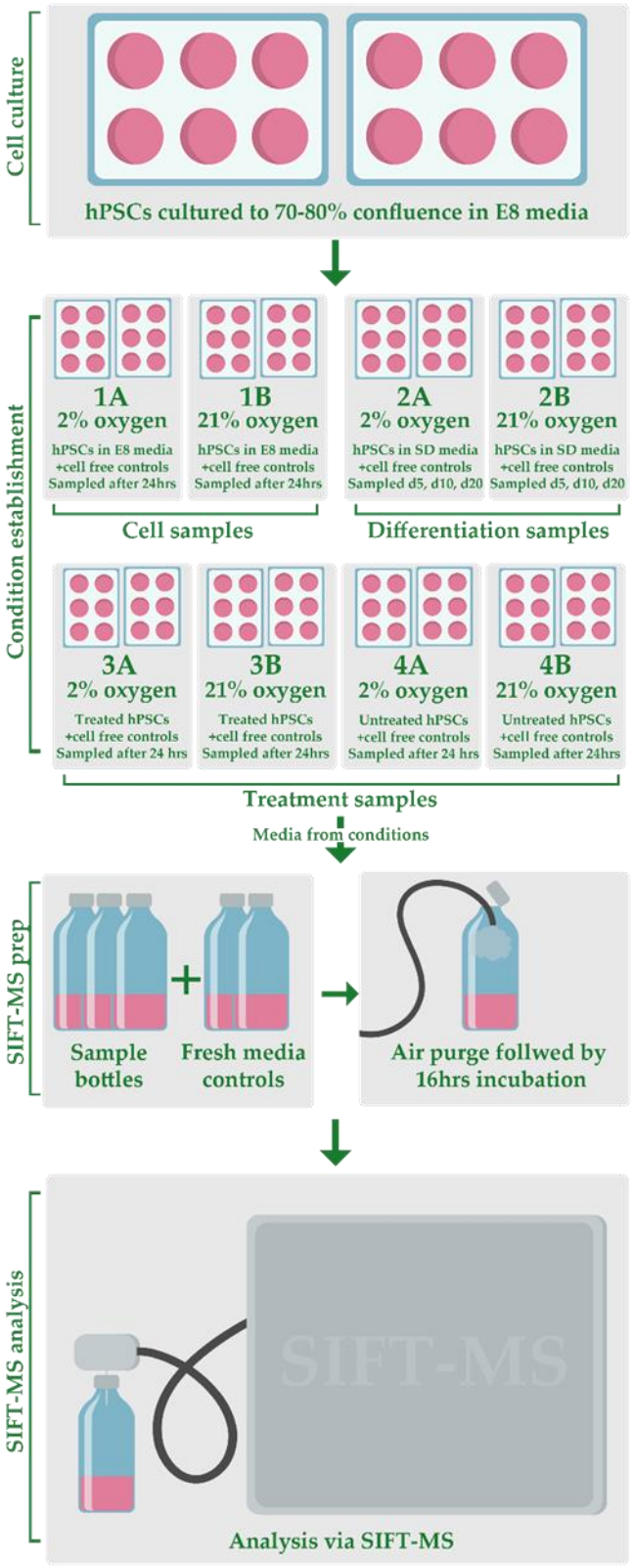

Figure 1. Experimental design for SIFT-MS analysis. Cells were initially cultured in Essential 8 and vitronectin substrate until they reached 70-80% confluence. Four sets of cell samples were created and cultured at either 21% or 2% O_2 (1A-4B). Undifferentiated hPSCs cultured for 24 hours (1A and 1B) (n=5). Differentiation samples, (days 5, 10 and 20) (2A and 2B) (n=3). Treatment samples, ADH and CYP2E1 inhibitor 4-methyl pyrazole (4-MP) (n=3). Cell-free controls (n=5 for E8 controls, n=9 for SD controls). Preparation for SIFT-MS analysis involved transferring media samples into sterile 150 mL glass bottles, covered with an aluminum screw cap and a black rubber septum. Additional

 doi:10.20944/preprints202203.0143.v1

fresh media controls were created at this stage (n=3). The headspace of the glass bottles was then purged with dry and compressed air, followed by incubation for 16 hours at 37 °C. SIFT-MS measurements were then performed in all samples.

2.10. Data analysis

For SIFT-MS datasets obtained in MIM mode, the cell media samples were initially normalized by subtracting the corresponding cell-free media control samples. Following this, t-test (for hPSCs media) or one-way ANOVA and post-hoc Turkey (for hPSC differentiated media) were performed for each VOC.

SIFT-MS datasets obtained in FS mode were analyzed using multivariate statistical analysis using SIMCA 14.1 software (MKS Umetrics AB, Umeå, Sweden). An unsupervised Principal Component Analysis (PCA) was followed by a supervised orthogonal projection least squares discriminant analysis (OPLS-DA), using log transformation and unit variance (UV) scaling. ANOVA or t-test was also performed on the spectral data to identify significant variables (ions) in the different cell culture media and O_2 conditions. m/z 19 precursor ion (H_3O^+) and its isotopologues at m/z 20 and m/z 21, water clusters and their isotopologues at m/z 37, m/z 38, m/z 39, m/z 55, m/z 56, m/z 57, m/z 73, m/z 74, m/z 75 and m/z 91 [44–46], and any undetected ions (m/z with zero values) were removed when processing the data. Values of $p < 0.05$ were accepted as statistically significant.

3. Results

3.1. hPSCs expression of pluripotent markers is independent of oxygen condition

Live staining indicated that the hPSC lines used in this study were SSEA-4 and TRA-1-60 positive and SSEA-1 negative (Figure 2), typical of undifferentiated hPSCs [47,48]. Furthermore, expression was independent of O_2 concentration. Flow cytometry was consistent with live staining observations (Figure 3A). No significant differences in surface marker expression levels were noted for hPSCs cultured in either 2% or 21% O_2 (Figure 3B and Table 1). SHEF-1 were 99% and 98% SSEA-4$^+$, 76% and 70% TRA-1-60$^+$, 2.5% and 2.6% SSEA-1$^+$ for 2% and 21% O_2, respectively. SHEF-2 were 91% and 83% SSEA-4$^+$, 69% and 65% TRA-1-60$^+$, and 4% and 5% SSEA-1$^+$ for 2% and 21% O_2, respectively. ZK2012L were 92% and 91% SSEA-4$^+$, and 58% and 52% TRA-1-60$^+$, for 2% and 21% O_2, respectively, whereas the same number of cells were SSEA-1$^+$ for both O_2 conditions (6%).

Preprints (www.preprints.org) | NOT PEER-REVIEWED | Posted: 10 March 2022 doi:10.20944/preprints202203.0143.v1

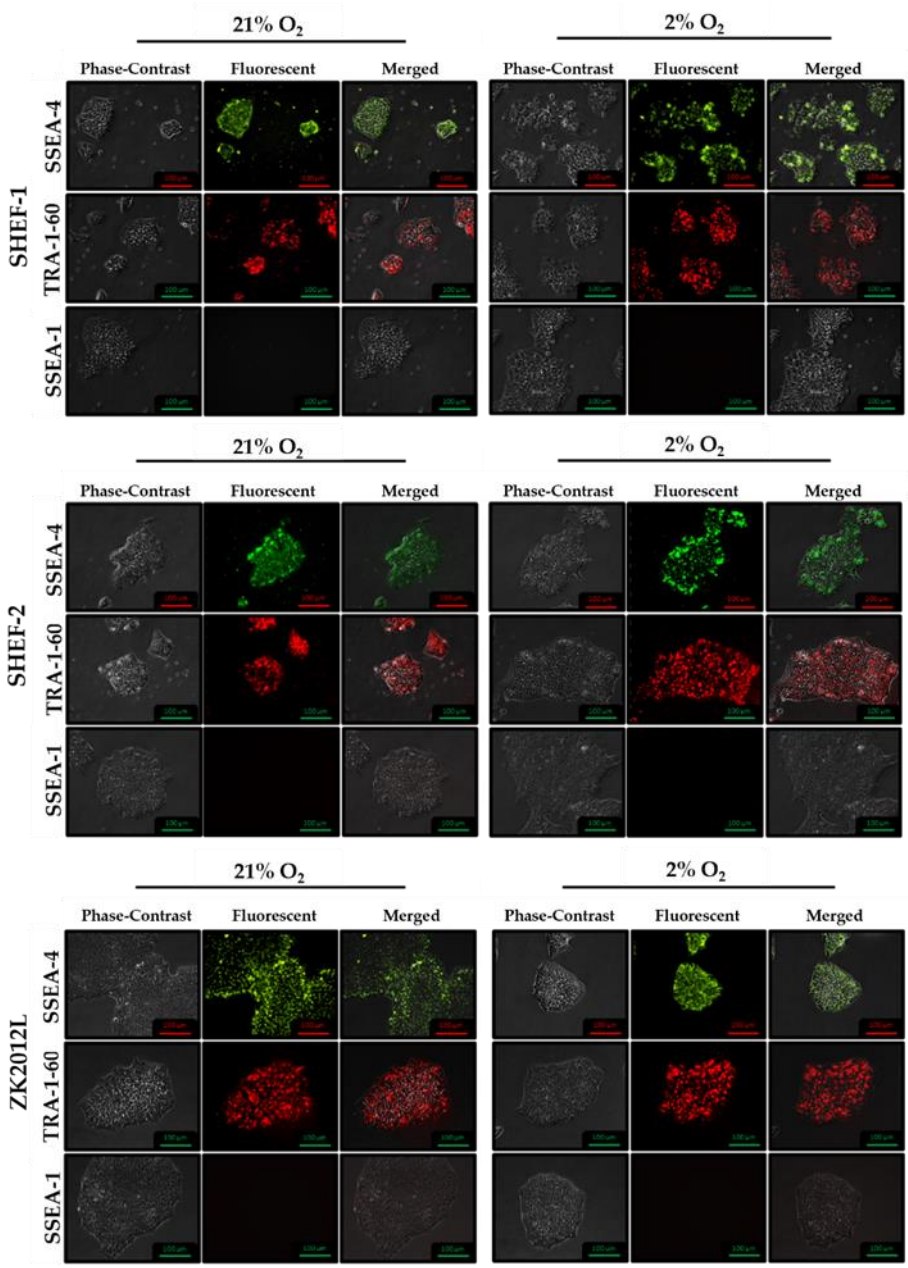

Figure 2. SSEA-4, TRA-1-60 and SSEA-1 expression in hPSCs. Phase-contrast (left column), fluorescent (middle column) and merged (right columns) images of SHEF-1, -2 and ZK2012L lines cultured in either 2% or 21% O_2. Scale bar is 100 μm.

Preprints (www.preprints.org) | NOT PEER-REVIEWED | Posted: 10 March 2022 doi:10.20944/preprints202203.0143.v1

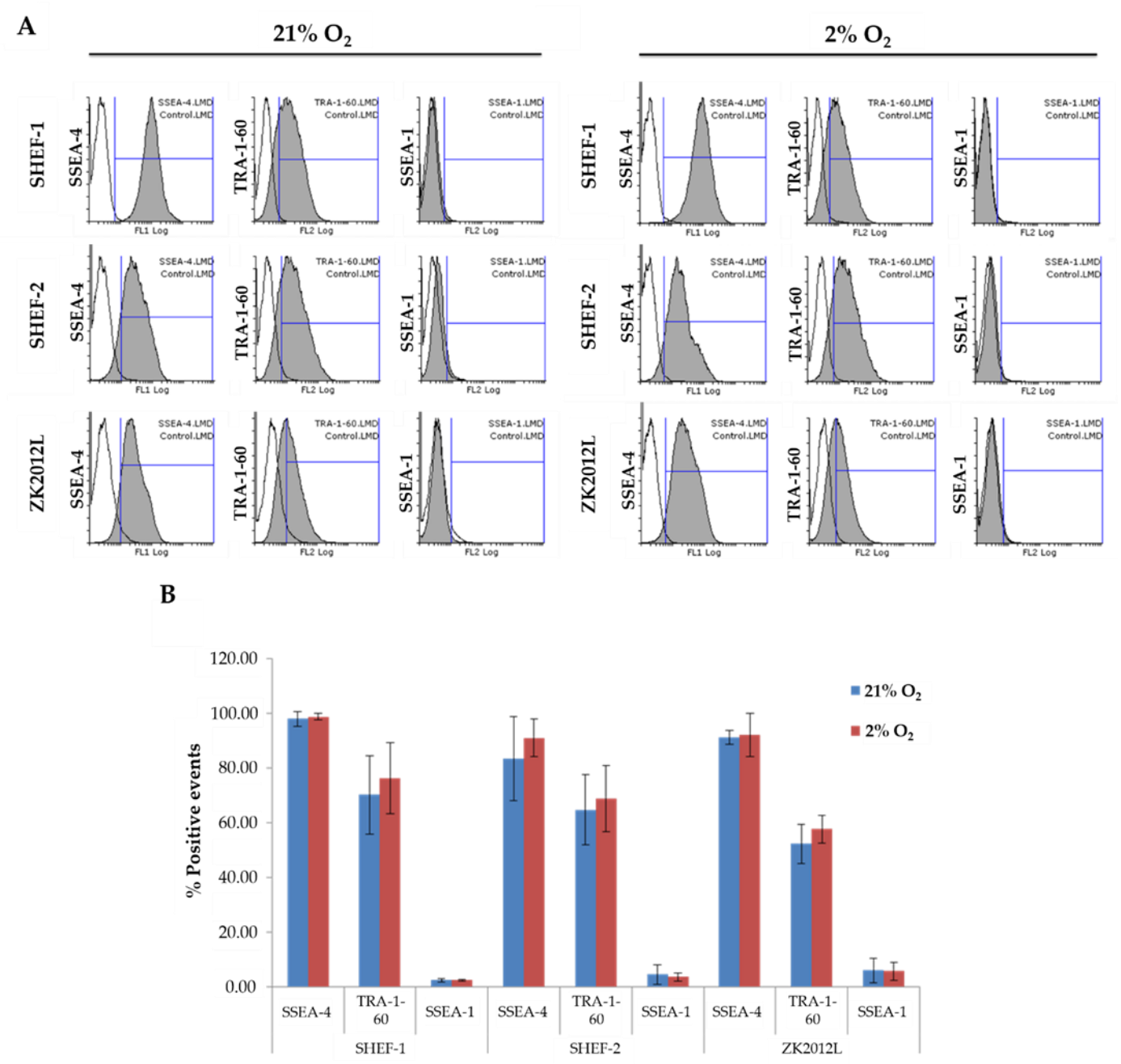

Figure 3. Flow cytometry analysis of SSEA-4, TRA-1-60 and SSEA-1 expression. (A) Histograms of SSEA-4, TRA-1-60 and SSEA-1 on SHEF-1, -2 and ZK2012L lines. (B) Percentage of positive cells for each marker in the two O_2 conditions.

Table 1. Percentages for the pluripotent markers SSEA-4 and TRA-1-60 and the differentiation marker SSEA-1 in the hPSC SHEF-1, SHEF-2 and ZK2012L by flow cytometry after 4 days in culture in 21% and 2% O_2.

	SHEF-1		SHEF-2		ZK2012L	
	Percentage of positive cells					
O_2 concentration	**21%**	**2%**	**21%**	**2%**	**21%**	**2%**
SSEA-4	97.9 ± 2.7	98.6 ± 1.2	83.4 ± 15.4	90.9 ± 6.9	91.1 ± 2.6	92.1 ± 7.9
TRA-1-60	70.2 ± 14.4	76.2 ± 12.9	64.7 ± 12.9	68.8 ± 12.0	52.3 ± 7.1	57.6 ± 5.1
SSEA-1	2.6 ± 0.6	2.5 ± 0.3	4.5 ± 3.7	3.74 ± 1.5	6.1 ± 4.5	5.8 ± 3.3

Preprints (www.preprints.org) | NOT PEER-REVIEWED | Posted: 10 March 2022 doi:10.20944/preprints202203.0143.v1

3.2. Pluripotent- and germ layer-specific markers expression levels change with differentiation and O_2 condition

Expression of the germ layer-specific markers AFP (endoderm), Brachyury (mesoderm) and OTX2 (ectoderm) was investigated in each cell line and for each O_2 condition. Generally, AFP gradually increased throughout differentiation for all hPSCs cultured in 21% O_2 and SHEF-1 in 2%. In contrast, SHEF-2 and ZK2012L in 2% O_2 showed a progressive rise of AFP expression until day 10 of differentiation, which then dropped to negligible levels at day 20. Brachyury expression profiles were distinct for each hPSC line and O_2 condition. In SHEF-1 cultured at 21%, Brachyury level was maximal at day 5 of differentiation, and it subsequently decreased to a barely visible level at day 20. In 2%, Brachyury reached its maximum expression by day 10 and subsequently decreased. This pattern was also observed for SHEF-2 in both O_2 conditions. However, cells in 2% displayed extremely faint levels of Brachyury expression. In ZK2012L cultured in 21%, Brachyury was not detected until day 20. Conversely, ZK2012L in 2% started expressing Brachyury by day 10, which reached its maximum at day 20. OTX2 expression was detected throughout the whole differentiation period in all hPSCs and O_2 conditions. In SHEF-1, decreased OTX2 was observed at day 20 for either O_2, whereas the reverse was seen for SHEF-2, in which the expression was lower at day 0. OTX2 was expressed at similar levels at all time points in ZK2012L for both O_2 conditions.

Immunofluorescence demonstrated that both POU5F1 and NANOG decreased in a time-dependent manner with differentiation (Figure 5). Their expression was maximal in hPSCs at day 0 of differentiation cultured in either O_2. ALP (Alkaline Phosphatase) and SSEA-4 showed similar expression patterns. Overall, there was a noticeable reduction in expression after 5 days of differentiation for all markers in hPSCs cultured in both O_2 conditions. Additionally, the level of fluorescence intensity seems to be maintained until day 10, and then is subsequently lost by day 20.

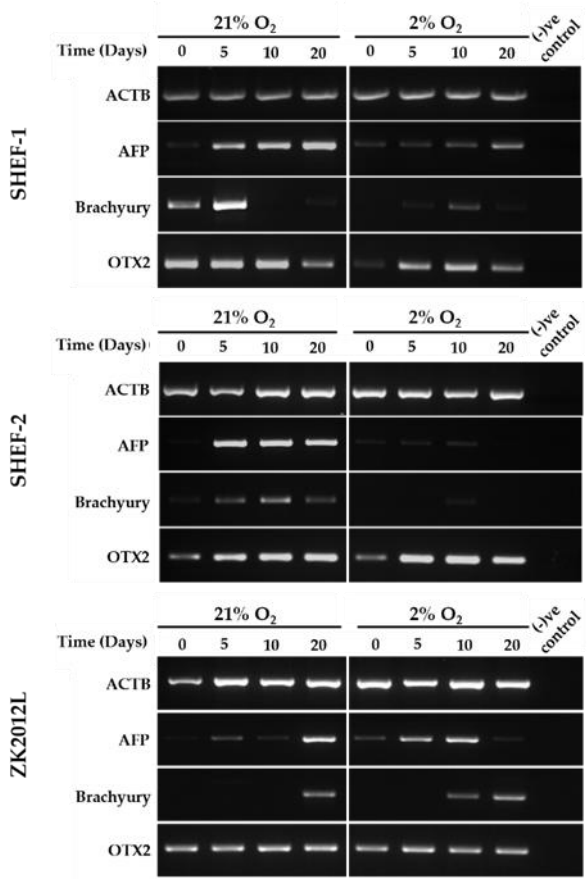

Preprints (www.preprints.org) | NOT PEER-REVIEWED | Posted: 10 March 2022 doi:10.20944/preprints202203.0143.v1

Figure 4. Expression of germ layer-specific gene markers at days 0, 5, 10 and 20 of differentiation. ACTB was used as a positive control. The differentiation markers AFP, Brachyury and OTX2 were used to assess differentiation toward the three germ layers: endoderm, mesoderm, and ectoderm, respectively.

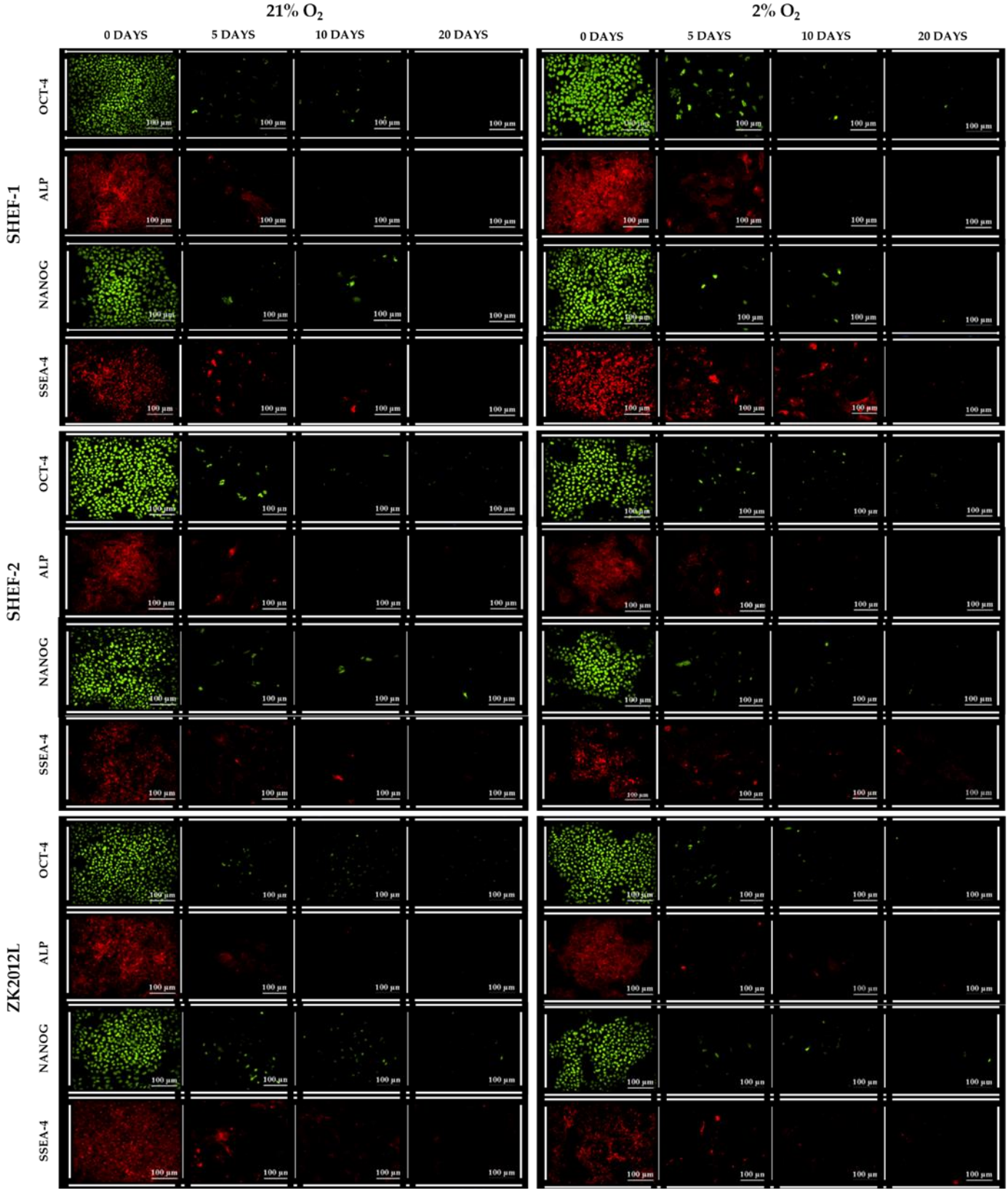

Figure 5. Expression of the pluripotency markers OCT4 (POU5F1, green), ALP (alkaline phosphatase, red), NANOG (green) and SSEA-4 (red) throughout hPSC differentiation. Expression levels were observed at specific time points of

Preprints (www.preprints.org) | NOT PEER-REVIEWED | Posted: 10 March 2022 doi:10.20944/preprints202203.0143.v1

differentiation (days 0, 5, 10 and 20) in the three hPSC lines (hESC SHEF-1 and -2, and hiPSC ZK2012L) cultured in 21% and 2% O_2. hPSCs were stained for Scale bar is 100 μm.

3.3. SIFT-MS can distinguish between media, undifferentiated hPSCs and hPSCs undergoing differentiation

PCA scores of most samples cultured in either O_2 condition are present within the plot of a 95% confidence region (Hotelling T2 ellipse) (Figure 6). Exceptions included some replicates from undifferentiated hPSC media samples, which were located outside of the confidence region. Across all score plots there is distinct clustering of control media samples (UNDIFF MED and DIFF MED). Day 0/undifferentiated hPSCs score plots for both SHEF-1 (Figure 6B) and SHEF-2 (Figure 6D) under 2% O_2 showed a tighter clustering than their 21% equivalents (Figure 6A and 6C). Differentiated samples (days 5, 10, and 20) demonstrated clear clustering, with day 20 samples being the tightest clustered group (Figure 6A - D). Some differentiated sample groups had clustering with overlap (SHEF-1 in 2% and SHEF-2 in 21%). There was no clear clustering of samples in the scores plots of ZK2012L (Figure 6E and 6F).

In all OPLS-DA models, the data lay within a 95% confidence region (Hotelling T2 ellipse) (Figure 7). Control media samples were clustered, with some overlap for both SHEF-1 and ZK2012L (Figure 7B and 7F). In contrast, SHEF-2 showed a more noticeable separation of each control media group (Figure 7C and 7D). Undifferentiated hPSCs (0 DAY) were tightly clustered and evidently separated from differentiation samples. This separation was greatest in SHEF-1 samples (Figure 7A and 7B), followed by SHEF-2 (Figure 7C and 7D) and then ZK2012L (Figure 7E and 7F). Overall, differentiation sample groups (5, 10, and 20 DAYS) showed tight clustering and clear separation across all samples. Exceptions included 2% Day 10 and Day 20 samples, which displayed some overlap for both SHEF-1 and ZK2012L (Figure 7B and 7F). Additionally, ZK2012L in 21% showed the most scattering of Day 5 and 10 samples compared to the rest of the samples (Figure 7E).

Preprints (www.preprints.org) | NOT PEER-REVIEWED | Posted: 10 March 2022 doi:10.20944/preprints202203.0143.v1

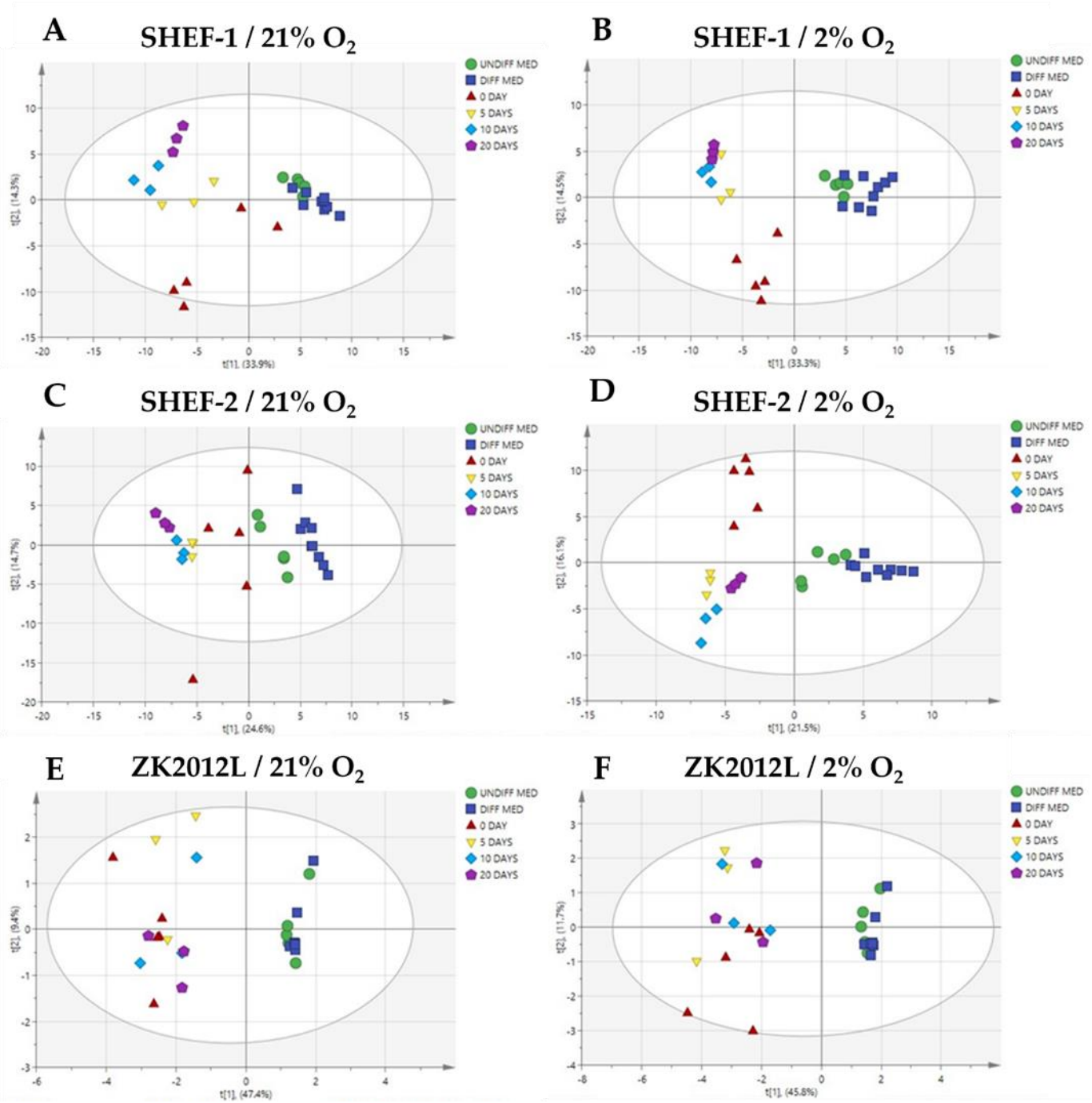

Figure 6. PCA score plots of hPSCs exposed culture media headspace. **(A)** SHEF-1 in 21% O_2 (t[1]=33.9%, t[2]=14.3%). **(B)** SHEF-1 in 2% O_2 (t[1]=33.3%, t[2]=14.5%). **(C)** SHEF-2 in 21% O_2 (t[1]=24.6%, t[2]=14.7%). **(D)** SHEF-2 in 2% O_2 (t[1]=21.5%, t[2]=16.1%). **(E)** ZK2012L in 21% O_2 (t[1]=9.4%, t[2]=47.4%). **(F)** ZK2012L in 2% O_2 (t[1]=11.7%, t[2]=45.8%). For each score plot, X and Y axes represent the first and second principal components, respectively. Ellipses represent the 95% confidence intervals for each PCA score plot. The control undifferentiated media (undiff med/E8 media) (n=5), differentiation media (diff med/Spontaneous Differentiation Media) (n=9) are shown as circles and squares, respectively, whereas day 0 undifferentiated cells media, day 5 differentiated cell media, day 10 differentiated cell media and day 20 differentiated cell media are shown as triangles inverted triangles, diamonds, and pentagons, respectively.

Preprints (www.preprints.org) | NOT PEER-REVIEWED | Posted: 10 March 2022 doi:10.20944/preprints202203.0143.v1

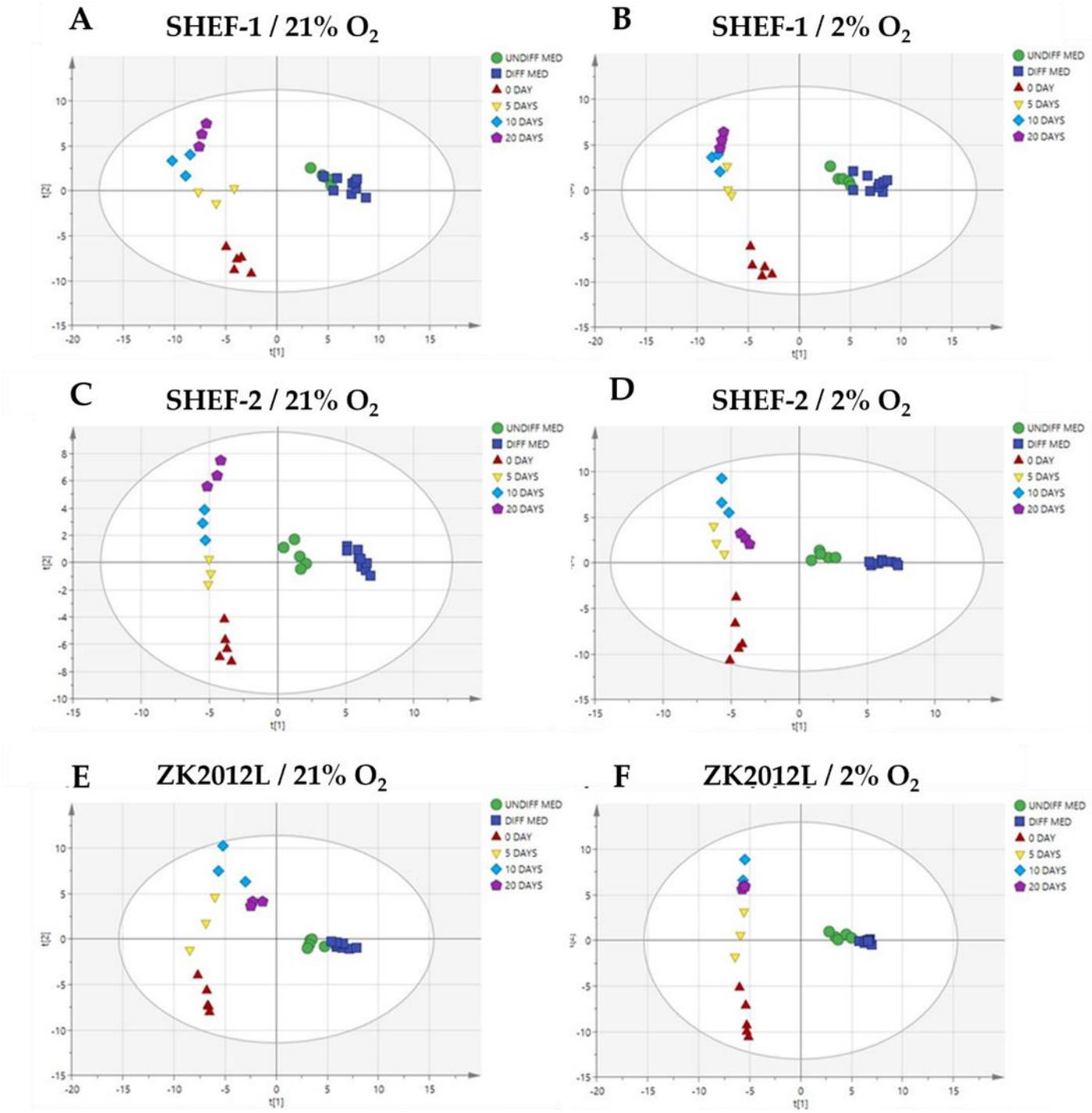

Figure 7. Scores plot from the OPLS-DA discrimination of SIFT-MS spectra. (A) SHEF-1 in 21% O_2 score plot, R^2Y(cum), Q^2(cum). (B) SHEF-1 in 2% O_2 score plot, R^2Y(cum), Q^2(cum). (C) SHEF-2 in 21% O_2 score plot, R^2Y(cum), Q^2(cum). (D) SHEF-2 in 2% O_2 score plot, R^2Y(cum), Q^2(cum). (E) ZK2012L in 21% O_2 score plot, R^2Y(cum), Q^2(cum). (F) ZK2012L in 2% O_2 score plot, R^2Y(cum), Q^2(cum). For each score plot, X-axis, t[1], and Y-axis, t[2], represent the first and second principal components, respectively. Ellipses represent the 95% confidence intervals for each OPLS-DA score plot. The control un-differentiated media (undiff med/E8 media) (n=5), differentiation media (diff med/Spontaneous Differentiation Media) (n=9) are shown as circles and squares, respectively. Day 0 undifferentiated cells media, day 5 differentiated cell media, day 10 differentiated cell media and day 20 differentiated cell media are shown as triangles, inverted triangles, diamonds and pentagons, respectively.

Preprints (www.preprints.org) | NOT PEER-REVIEWED | Posted: 10 March 2022 doi:10.20944/preprints202203.0143.v1

3.4. MIM mode detects different VOC levels in undifferentiated hPSCs cultured in distinct O_2 conditions

The concentration levels of 10 VOCs (acetone, acetaldehyde, ethanol, butanol, pentanol, hexanal, DMS/ethanethiol, butyric acid, pentene and putresceine) in the headspace of hPSCs media were analyzed using the MIM mode of SIFT-MS (Table 2). Acetone was present at similar levels in all hPSCs irrespective of the O_2 condition. 2% O_2 led to an increase in VOC levels for acetaldehyde, DMS/ethanethiol and putresceine compared to 21% for two hPSC lines (SHEF-2 and ZK2012L for acetaldehyde and DMS/ethanethiol, and SHEF-1 and ZK2012L for putresceine), which was significant for both acetaldehyde and DMS/ethanethiol. In contrast, 21% O_2 caused two hPSC populations to release higher amounts of both butanol and hexanal compared to 2% (SHEF-2 and ZK2012L, and SHEF-1 and SHEF-2, respectively). SHEF-2 and ZK2012L at 2% showed a decrease/consumption of butanol, whereas most samples exhibited neither an increase nor a decrease in hexanal levels. Ethanol was released at similar levels for most conditions (exception of ZK2012L at 2%), and this release was significant for SHEF-1 regardless of O_2 condition. Pentanol was present at comparable concentrations in most hPSCs and O_2 conditions. Exceptions included both SHEF-2 at 21% and ZK2012L at 2%, which released a higher amount of pentanol. Butyric acid was present at similar levels in most hPSCs regardless of the O_2 condition, except for ZK2012L at 21%, which displayed a lower increase of butyric acid level. Each hPSC line exhibited distinct patterns for pentene. SHEF-1 presented comparable levels of pentene in either O_2 condition, whereas the other hPSCs showed a higher VOC release than SHEF-1 (SHEF-2 at 21% and ZK2012L at 2%) and VOC consumption/decrease (SHEF-2 at 2% and ZK2012L at 21%).

Table 2. Quantification of VOCs in the headspace of hPSCs using H_3O^+ precursor in MIM mode.

	SHEF-1		SHEF-2		ZK2012L	
O_2 concentration	**21%**	**2%**	**21%**	**2%**	**21%**	**2%**
Acetone	+	+	+	+	+	+
Acetaldehyde	+	+	+*	++*	+*	++*
Ethanol	+*	+*	+	+	+	x
Butanol	++	+	++	-	++	-
Pentanol	+	+	++	+	+	++
Hexanal	+	x	+	x	x	x
DMS/Ethanethiol	++	++	+*	++*	+*	++*
Butyric Acid	++	++	++	++	+	++
Pentene	+	+	++	-	-	++
Putresceine	+	++	+	+	+	++

* Statistically different ($p<0.05$) between 21% O_2 and 2% O_2 conditions. DMS: Dimethyl sulfide. (x) means absence of compound, (+) means some increase/release of compound, (++) means high increase/release of compound, (-) means decrease/consumption of compound.

3.5. MIM mode detects different VOC levels in hPSCs undergoing differentiation in distinct O_2 conditions

The same VOCs were also analyzed in the headspace of hPSCs media during specific time points of hPSC differentiation in either 2% or 21% O_2 (Table 3). In SHEF-1, most VOCs showed a decrease in concentration from day 0 to day 5 of differentiation, followed by an increase until day 10, to their maximal level, before a further decline from day 10 to day 20, where values were lowest (except for hexanal at 2%). This trend was also more noticeable for most VOCs (acetone, ethanol, butanol, hexanal, butyric acid, pentene and putresceine) in cells cultured in 21%. Exceptions included acetaldehyde and DMS/ethanethiol at

Preprints (www.preprints.org) | NOT PEER-REVIEWED | Posted: 10 March 2022 doi:10.20944/preprints202203.0143.v1

both O_2 conditions and ethanol at 2%. Both acetaldehyde and DMS/ethanethiol significantly dropped after 5 days ($p<0.01$) and were maintained throughout the rest of the differentiation process. In contrast, ethanol in SHEF-1 at 2% was present at similar levels throughout the entire period.

In SHEF-2 different patterns of VOC concentration could be observed throughout differentiation. Many VOCs exhibited a decrease in concentration from day 0 to day 5 of differentiation, followed by an increase until day 10 and a further decline from day 10 to day 20. VOCs showing this pattern included ethanol and hexanal at both O_2 conditions, pentanol, butyric acid, and putresceine at 2% and butanol at 21%. Acetone in both conditions and putresceine at 21% displayed the reverse, increasing from day 0 to 5 (reaching the highest levels), decreasing until day 10 (where it was lowest) and then rising until day 20. Like SHEF-1, both acetaldehyde and DMS/ethanethiol significantly dropped after 5 days ($p<0.01$) and were maintained throughout the rest of the differentiation process. Butanol and pentene levels in 2% continuously raised until day 10, followed by a decline. The opposite was observed for pentanol and butyric acid at 21%. Finally, pentene at 21% showed a unique pattern where it decreased over the first 5 days and then continuously increased until the end of differentiation.

In ZK2012L, each O_2 condition displayed different concentration changes across differentiation for each VOC, with the exceptions of acetone and pentene. These VOCs decreased in the first 5 days and then elevated until day 10. The differences occurred after day 10, where acetone decreased, and pentene continued to increase until day 20. Once again, both acetaldehyde and DMS/ethanethiol showed similar concentration level patterns across differentiation and between each O_2 condition. In 21%, both VOCs gradually decreased throughout differentiation, which was significant ($p<0.01$), whereas at 2%, the VOC levels progressively declined until day 10 and then increased up to day 20. Both ethanol and hexanal exhibited similar concentration profiles for both O_2 conditions. The VOCs gradually elevated throughout differentiation in cells at 2%, with the changes in ethanol being significantly different ($p<0.05$). In contrast, 21% profiles showed a decline until day 5, followed by a rise from day 5 to day 20. Comparable VOC patterns were also observed for both pentanol and butyric acid. In these VOCs, concentrations gradually increased throughout differentiation in 21%, while a decline was seen in the first 10 days, which was followed by a rise until day 20. Butanol was maintained at similar levels during differentiation of ZK2012L at 2%, and this profile was also observed for putresceine at 21%. For butanol at 21%, there was a decrease from day 0 to day 5, followed by an increase and then another decline. In contrast, putresceine progressively decreased until day 10 and then elevated toward the end of differentiation.

Overall, the effects of O_2 tension on VOC production/consumption during differentiation were minor on SHEF-1, with only ethanol, hexanal and putresceine showing different trends at 21% and 2%. VOC concentrations in SHEF-2 were more affected by O_2 compared to SHEF-1 (six VOCs fluctuated distinctly compared to the three observed in SHEF-1). O_2 had the greatest effect on ZK2012L, which showed different trends for almost all VOCs at 2% and 21%. The only exception was acetaldehyde, showing a relatively similar production/consumption trend during differentiation irrespective of O_2 condition.

Preprints (www.preprints.org) | NOT PEER-REVIEWED | Posted: 10 March 2022 doi:10.20944/preprints202203.0143.v1

Table 3. Quantification of VOCs in the headspace of hPSCs and their progeny using H_3O^+ precursor in MIM mode.

	SHEF-1								SHEF-2								ZK2012L							
O_2 concentration	**21%**				**2%**				**21%**				**2%**				**21%**				**2%**			
Time Point (days)	**0**	**5**	**10**	**20**	**0**	**5**	**10**	**20**	**0**	**5**	**10**	**20**	**0**	**5**	**10**	**20**	**0**	**5**	**10**	**20**	**0**	**5**	**10**	**20**
Acetone	+	-	+	--	+	-	+	--	+	++	+	+	+	++	+	++	+	-	+	+	+	--	-	---
Acetaldehyde	++	+*	+*	+*	++	+*	+*	+*	++	-*	-*	-*	++	-*	-*	-*	+	+*	+*	+*	+	+	-	+
Ethanol	++	+	++	+	+	+	+	+	+	-	+	-	+	-	+	-	+	-	+	+	+	+	++	++
Butanol	++	+	++	--	+	+	+	--	+	-	+	-	--	-	+	-	+	--	+	-	-	-	-	-
Pentanol	+	+	++	-	+	+	+	--	+	-	--	+	+	-	+	-	+	+	++	++	+	-	--	-
Hexanal	++	-	++	-	+	-	-	-	++	+	++	+	+	+	+	-	-	--	-	+	+	+	++	++
DMS/Ethanethiol	++	+*	+*	+*	++	+*	+*	+*	+	-*	-*	-*	++	-*	-*	-*	+	+*	+*	+*	++	+	--	+
Butyric Acid	+	+	++	--	+	+	+	--	+	-	--	+	+	--	-	-	+	++	++	++	+	-	--	-
Pentene	++	+	++	+	++	+	++	-	+	--	--	-	-	-	+	-	-	--	-	+	+	--	-	-*
Putresceine	+	-	++	-	+	+	++	--	+	+	--	-	+	-	+	-	+	+	+	+	+	+	--	-

* Statistically different ($p<0.05$) between 21% O_2 and 2% O_2 conditions. DMS: Dimethyl sulfide. (+) means some increase/release of compound, (++) means high increase/release of compound, (-) means decrease/consumption of compound, (--) means high decrease/consumption of compound.

3.6. The acetaldehyde profile detected by SIFT-MS is an indicator of self-renewal and differentiation in hPSCs

Undifferentiated hPSCs exhibited significantly increased acetaldehyde compared to their differentiating counterparts, which was more apparent in 2% O_2. Acetaldehyde is an intermediate metabolite of ethanol metabolism [49,50]. Ethanol is oxidized to acetaldehyde by the enzymes alcohol dehydrogenase (ADH), cytochrome P450 family 2 subfamily E member 1 (CYP2E1), or catalase (CAT) [49]. Acetaldehyde is then further oxidized to acetate by aldehyde dehydrogenases (ALDH) [49]. We next determined expression levels of genes involved in ethanol metabolism to establish whether the levels of acetaldehyde detected by SIFT-MS associated with ethanol metabolism in hPSCs. Genes encoding enzymes implicated in various stages of ethanol metabolism were selected (Figure S1) for expression analysis.

Previous reports have demonstrated that 2% O_2 upregulates genes involved in signaling pathways and metabolism in hESCs via microarray bioinformatics analysis [51]. This microarray data was reanalyzed to identify if ethanol metabolism-related enzymes were differentially expressed in hESCs at 2%. The genes CAT, CYP2E1, ADH4, ADH5, ALDH1L2, and ALDH18A1 were upregulated, whereas ALDH9A1, ALDH4A1, ALDH7A1, ALDH16A1, ALDH1B1, ALDH1A2, ALDH3A2, ALDH5A1, ALDH6A1, ALDH1A3, ALDH1A1 were downregulated (Figure 8A). From this gene list, 6 genes (ADH4, ADH5, CYP2E1, ALDH1A1, ALDH1A3 and ALDH6A1) were selected for further transcriptional analysis to confirm if these changes were also observed in SHEF-1, SHEF-2 and ZK2012L. RT-PCR indicated hPSC upregulation of ADH4, ADH5, and CYP2E1 and downregulation of ALDH1A1, ALDH1A3, and ALDH6A1 in 2% O_2 (Figure 8B).

Chemical knockdown of ADH and CYP2E1 using 4-MP was performed to validate the observed changes in acetaldehyde from SIFT-MS (Figure 8C and 8D). Following establishment of non-toxic 4-MP dosage (5 mM, Figure S2), hPSCs were maintained in 4-MP, and levels of ethanol and acetaldehyde in the media headspace determined. 4-MP addition resulted in increased ethanol levels in hPSCs at both 21% and 2% O_2. In contrast, acetaldehyde levels decreased in the majority of treated cultures. This reduction achieved significance for hiPSCs in 21% ($p<0.01$).

Preprints (www.preprints.org) | NOT PEER-REVIEWED | Posted: 10 March 2022 doi:10.20944/preprints202203.0143.v1

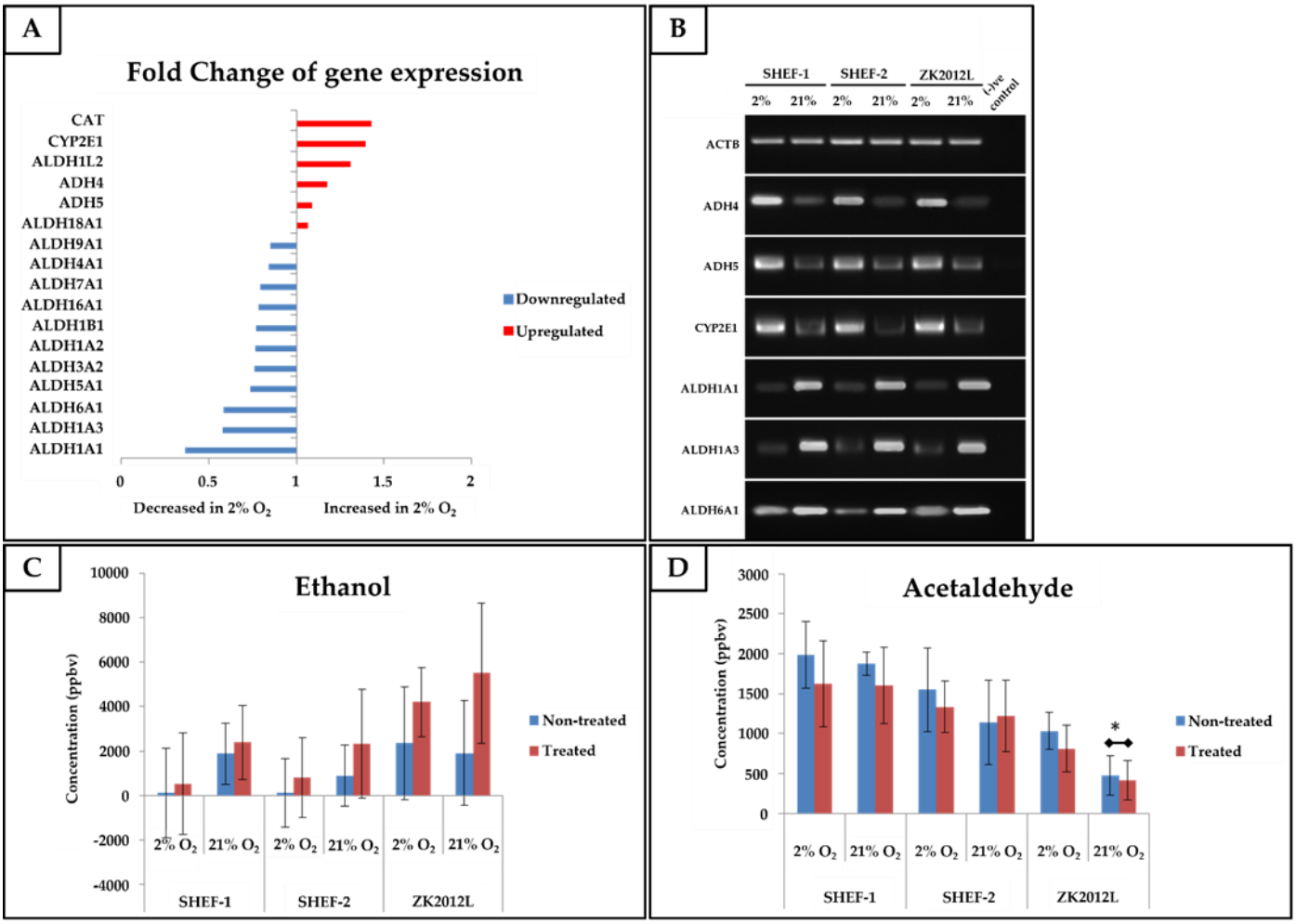

Figure 8. Ethanol metabolism activity in hPSCs assessed by molecular and SIFT-MS techniques. (A) Fold-change in microarray gene expression level in hPSCs was plotted on scale 0 to 2 [>1 for upregulation (red bars), <1 for downregulation (blue bars)]. (B) RT-PCR of selected genes involved in ethanol metabolism. ACTB was used as positive control. (C-D) Treatment with the ADH/CYP2E1 inhibitor 4-methyl pyrazole (4-MP) led to changes in the concentrations of ethanol (C) and acetaldehyde (D) in the headspace of hPSC media. Y-axis represents part-per-billion by volume (ppbv) measured in the headspace of samples of non-treated cells (blue bars) and cells treated with 5 mM 4-MP (red bars). X-axis shows the hPSC lines tested (SHEF-1, SHEF-2 and ZK20212L) cultured in both 2% O_2 and 21% O_2. Error bars represent +/-SD. Asterisk indicates significant difference ($p<0.01$) between non-treated and 4-MP treated samples.

4. Discussion

Here we demonstrate, in a first of its kind study, that SIFT-MS is effective in identification and quantification of VOCs in hPSCs and their differentiating lineages. Alternate technologies utilized in detection of VOCs in hPSCs include Solid-Phase Microextraction/Gas Chromatography/Mass Spectrometry (SPME/GC-MS) and electronic nose (e-nose) [35]. GC-MS is the gold standard approach to detect VOCs due to its reproducibility and high sensitivity [52]. Unfortunately, CG-MS does not allow for real-time analysis (usually requiring complicated sample preparation) [40], is invasive, and labor-intensive [53]. e-nose can detect VOCs with high efficiency coupled to simplicity of operation [54]. In contrast to GC-MS, e-nose is non-destructive, however, utility is diminished as sensors can be toxic to cells and have limited sensitivity [55]. SIFT-MS overcomes many of these limitations with high sensitivity, non-invasive application, and ease of use, with no requirement for sample preparation [40]. Because of these advantages, SIFT-MS has the potential to be used in clinical medicine and cell manufacturing as a monitoring device.

We did not detect any significant effects of different O_2 conditions in the expression of pluripotency markers. Immunostaining of germ layer markers also demonstrated no

 doi:10.20944/preprints202203.0143.v1

major differences in expression during differentiation at 2% and 21% O_2. In contrast, both hPSC proliferation and mitochondrial activity were affected by O_2 (Figure S3). 2% lead to increased proliferation and mitochondrial activity in SHEF-1, and a similar rise was also noticed for SHEF-2 and ZK2012L at 21%. These observations are consistent with previous studies in which distinct O_2 conditions did not lead to alterations in pluripotent and differentiation marker expression while changes in their metabolic states were observed [17–19,56]. However, hPSC proliferation and mitochondrial activity in this study appeared hPSC line specific, indicating inherent variability likely due to interline differences that result in distinct hPSC behavior, stability, and quality [2,57–61]. Additionally, the chosen molecular techniques to assess cellular metabolism are limited in the information they can provide since hPSCs rely on glycolysis for energy production [17–19,62–65]. Therefore, further studies incorporating approaches that analyze glucose consumption and lactate production, such as glucose and L-lactate detection assays, may potentially clarify the results obtained in this study.

Germ layer genes were expressed differently during differentiation at both O_2 conditions. In SHEF lines, 2% O_2 generally led to a downregulation of germ layer genes (AFP and Brachyury) compared to 21%. Previous studies have demonstrated that low oxygen levels result in a decrease propensity for endodermal and mesodermal formation during differentiation [66,67]. In contrast, no evident difference in expression pattern for OTX2 was observed between the two O_2 conditions, which follows the results of a previous study [18]. However, other studies have shown that mesoderm [68–70] and ectoderm [71,72] are promoted, whereas endoderm is suppressed in low O_2 conditions [73]. Further quantification of the genes used in this study will clarify the effects of different O_2 conditions on germ layer gene expression.

PCA allows for the identification of variance (differences) between the measurements collected from analytical chemistry techniques such as mass spectrometry [74]. Here, we sought to identify a set of metabolites associated with media-only, undifferentiated or differentiating hPSCs, and whose concentration would alter with the O_2 condition. PCA scores positioned media-only samples into distinct clusters from the other groups. We reasoned that the absence of group separation with undifferentiated and differentiating hPSCs could potentially be due to the high variability present in the samples [74]. To assess this variability, OPLS-DA models were applied, which revealed group separation between all samples. Differentiating samples formed clusters close to each other, and these were separated from undifferentiated hPSCs. This demonstrated that undifferentiated hPSCs have distinct VOC profiles from their differentiating counterparts.

SIFT-MS MIM mode allows accurate and precise quantification of specific VOCs [75] where the outputs are time profile specific for each selected VOC. MIM data indicated that the majority of VOCs analyzed were detected at different concentrations in the two O_2 conditions. Overall, no clear pattern in the VOC profiles of undifferentiated and differentiating hPSCs emerged. VOC generation was cell line dependent with specific concentrations, timepoints and O_2 conditions. The inherent variability present between different hPSC lines, which, in turn, leads to variation in differentiation capacity, may be responsible for this absence of typical features [60,61,76,77]. Further, it may be that future refinement of experiments and addition of other analytical chemistry techniques, such as GC-MS [35,78], raman spectroscopy [79–84] or synchrotron Fourier transform infrared (FTIR) [79,85], are required to clarify and validate the SIFT-MS observations.

A general observation was the significant decrease of both acetaldehyde and DMS/ethanethiol once differentiation was initiated. Acetaldehyde has been detected in various cancer cell lines at concentrations of 100-1500 ppb [86–89]. hPSCs and cancer cells have a similar metabolism to support unlimited proliferation [26,90,91] and thus, acetaldehyde might have roles in maintaining self-renewal. For instance, both cell types favor glycolysis over oxidative phosphorylation to produce energy even if they contain functional mitochondria and there is sufficient oxygen to support mitochondrial respiration [23,25,26]. A reason for this could be the hypoxic environment where cells reside, as seen

 doi:10.20944/preprints202203.0143.v1

for hematopoietic stem cells [92,93] and cancer cells [90,94,95]. This study showed that lower O_2 conditions (2%) upregulated expression of enzymes participating in the conversion of ethanol to acetaldehyde (ADH4, ADH5, and CYP2E1) while downregulating enzymes involved in generating acetate from acetaldehyde (ALDH1A1, ALDH1A3, and ALDH6A1). In contrast, the opposite was observed for 21% O_2. It is possible that low oxygen, known to stimulate a more undifferentiated state in hPSCs [5,8,9,13–16], promotes the generation of acetaldehyde, which, in turn, may contribute to the maintenance of pluripotency and self-renewal in hPSCs.

Further, DMS displays antioxidant properties, providing cells with protection against free radical DNA damage and enabling cell longevity [96]. When considered alongside that the long-term culture of hPSCs can result in the appearance of chromosomal abnormalities [5–8], we propose that high concentrations of DMS may form a component of a feedback loop driving genomic stability in long-term culture.

SIFT-MS analyses the cellular exometabolome, which reflects the intracellular metabolism [97,98]. Therefore, a way to understand which intracellular metabolic pathways contribute to the exometabolome is to introduce modifications either intra- or extra-cellularly [98]. Application of chemical inhibitors or inducers can change the activity of intracellular metabolic pathways, which, in turn, might alter the composition of the exometabolome. With this in mind, the current study also investigated whether ethanol metabolism is active in hPSCs since acetaldehyde was detected at higher concentrations in undifferentiated hPSCs. Supplementation with an inhibitor that interferes with the oxidation of ethanol resulted in a rise in ethanol and a decrease in acetaldehyde concentrations. This observation coupled to the transcriptional changes indicate that ethanol metabolism is likely to be an active metabolic pathway in hPSCs. Future steps should incorporate additional analytical chemistry methods to validate further and enhance confidence in the SIFT-MS results.

SIFT-MS demonstrated that O_2 concentration affects hPSC metabolism without obvious changes in self-renewal, pluripotency, and differentiation capacity. It is evident that improved understanding of the metabolic processes during the maintenance and differentiation of hPSCs is required before realizing the clinical and commercial potential of hPSCs. SIFT-MS is identified here as a technique that can assist in this realization by providing a non-destructive and timely analysis of the cell exometabolome.

5. Conclusions

hPSC behavior changes depending on the *in vitro* culture conditions, here, when O_2 concentrations vary. Because O_2 is inherently a critical factor in cellular metabolism and metabolism is closely linked to epigenetics and cell fates, it is imperative to accurately define the role of O_2 in intracellular metabolic pathways of hPSCs. SIFT-MS can be a vital contributor in revealing such roles through the study of VOC release. Combined with other omics approaches, this could reduce the gap between the metabolome and genome. Unfolding the metabolic processes occurring in hPSCs during maintenance and differentiation has potential to improved culture protocols and the development of new characterization assays that focus on the metabolism of hPSCs to ensure the maintenance of hPSCs in long-term culture.

Supplementary Materials: The following are available online at www.mdpi.com/xxx/s1, Table S1: Primer design and annealing temperature of the genes investigated in this study, Figure S1: Genes involved in ethanol metabolism that were selected for expression analysis, Figure S2: Viability of hPSCs exposed to different concentrations of the ADH and CYPE1 inhibitor 4-methyl pyrazole (4-MP) cultured in both 21% and 2% O_2, Figure S3: Influence of physioxia (2% O_2) and air oxygen (21% O_2) on the proliferation and metabolic activity of hPSCs.

Author Contributions: Conceptualization, S.B., M.A.A.-Z., N.R.F. and A.V.R.; methodology, M.A.A.-Z., T.P.D. and S.J.K.; formal analysis M.A.A.-Z. and S.B.; visualization S.B., A.J.W., N.R.F. and A.V.R.; writing—original draft preparation, S.B., and A.V.R.; writing—review and editing, S.B.,

T.P.D., Z.K., S.J.K., J.S.-S., N.R.F. and A.V.R.; supervision, N.R.F and J.S.-S. All authors have read and agreed to the published version of the manuscript.

Funding: This work was supported by Iraqi Ministry of Higher Education and Scientific Research (MO-HESR) to M.A.A-Z (S1268). This research was also funded by the Engineering and Physical Sciences Research Council (EPSRC), UK, grant number EP/L015072/1 and the APC was funded by Biomolecules.

Institutional Review Board Statement: Not applicable.

Informed Consent Statement: Not applicable.

Data Availability Statement: The study did not report data that need to be reported.

Acknowledgments: We would like to acknowledge Prof. Patrik Španěl and his group at The Heyrovský Institute of Physical Chemistry, Prague for providing a comprehensive kinetic library and their assistance in the maintenance of the SIFT-MS instrument.

Conflicts of Interest: The authors declare no conflict of interest. The funders had no role in the design of the study; in the collection, analyses, or interpretation of data; in the writing of the manuscript, or in the decision to publish the results.

References

1. Trounson, A.; DeWitt, N.D. Pluripotent Stem Cells Progressing to the Clinic. *Nat Rev Mol Cell Biol* **2016**, *17*, 194–200, doi:10.1038/nrm.2016.10.
2. Dakhore, S.; Nayer, B.; Hasegawa, K. Human Pluripotent Stem Cell Culture: Current Status, Challenges, and Advancement. *Stem Cells International* **2018**, *2018*, 1–17, doi:10.1155/2018/7396905.
3. Kropp, C.; Massai, D.; Zweigerdt, R. Progress and Challenges in Large-Scale Expansion of Human Pluripotent Stem Cells. *Process Biochemistry* **2017**, *59*, 244–254, doi:10.1016/j.procbio.2016.09.032.
4. Zweigerdt, R. Large Scale Production of Stem Cells and Their Derivatives. In *Engineering of Stem Cells*; Martin, U., Ed.; Springer Berlin Heidelberg: Berlin, Heidelberg, 2009; pp. 201–235 ISBN 978-3-540-88805-5.
5. Guo, C.-W.; Kawakatsu, M.; Idemitsu, M.; Urata, Y.; Goto, S.; Ono, Y.; Hamano, K.; Li, T.-S. Culture under Low Physiological Oxygen Conditions Improves the Stemness and Quality of Induced Pluripotent Stem Cells: GENOMIC STABILITY IN IPS CELLS. *J. Cell. Physiol.* **2013**, *228*, 2159–2166, doi:10.1002/jcp.24389.
6. Maitra, A.; Arking, D.E.; Shivapurkar, N.; Ikeda, M.; Stastny, V.; Kassauei, K.; Sui, G.; Cutler, D.J.; Liu, Y.; Brimble, S.N.; et al. Genomic Alterations in Cultured Human Embryonic Stem Cells. *Nat Genet* **2005**, *37*, 1099–1103, doi:10.1038/ng1631.
7. Baker, D.E.C.; Harrison, N.J.; Maltby, E.; Smith, K.; Moore, H.D.; Shaw, P.J.; Heath, P.R.; Holden, H.; Andrews, P.W. Adaptation to Culture of Human Embryonic Stem Cells and Oncogenesis in Vivo. *Nat Biotechnol* **2007**, *25*, 207–215, doi:10.1038/nbt1285.
8. Li, T.-S.; Marbán, E. Physiological Levels of Reactive Oxygen Species Are Required to Maintain Genomic Stability in Stem Cells. *STEM CELLS* **2010**, N/A-N/A, doi:10.1002/stem.438.
9. Thompson, O.; von Meyenn, F.; Hewitt, Z.; Alexander, J.; Wood, A.; Weightman, R.; Gregory, S.; Krueger, F.; Andrews, S.; Barbaric, I.; et al. Low Rates of Mutation in Clinical Grade Human Pluripotent Stem Cells under Different Culture Conditions. *Nat Commun* **2020**, *11*, 1528, doi:10.1038/s41467-020-15271-3.
10. Garitaonandia, I.; Amir, H.; Boscolo, F.S.; Wambua, G.K.; Schultheisz, H.L.; Sabatini, K.; Morey, R.; Waltz, S.; Wang, Y.-C.; Tran, H.; et al. Increased Risk of Genetic and Epigenetic Instability in Human Embryonic Stem Cells Associated with Specific Culture Conditions. *PLoS ONE* **2015**, *10*, e0118307, doi:10.1371/journal.pone.0118307.
11. Jacobs, K.; Zambelli, F.; Mertzanidou, A.; Smolders, I.; Geens, M.; Nguyen, H.T.; Barbé, L.; Sermon, K.; Spits, C. Higher-Density Culture in Human Embryonic Stem Cells Results in DNA Damage and Genome Instability. *Stem Cell Reports* **2016**, *6*, 330–341, doi:10.1016/j.stemcr.2016.01.015.
12. Ivanovic, Z. Hypoxia or in Situ Normoxia: The Stem Cell Paradigm. *J. Cell. Physiol.* **2009**, *219*, 271–275, doi:10.1002/jcp.21690.

13. Forsyth, N.R.; Musio, A.; Vezzoni, P.; Simpson, A.H.R.W.; Noble, B.S.; McWhir, J. Physiologic Oxygen Enhances Human Embryonic Stem Cell Clonal Recovery and Reduces Chromosomal Abnormalities. *Cloning and Stem Cells* **2006**, *8*, 16–23, doi:10.1089/clo.2006.8.16.
14. Ezashi, T.; Das, P.; Roberts, R.M. Low O2 Tensions and the Prevention of Differentiation of HES Cells. *Proceedings of the National Academy of Sciences* **2005**, *102*, 4783–4788, doi:10.1073/pnas.0501283102.
15. Prasad, S.M.; Czepiel, M.; Cetinkaya, C.; Smigielska, K.; Weli, S.C.; Lysdahl, H.; Gabrielsen, A.; Petersen, K.; Ehlers, N.; Fink, T.; et al. Continuous Hypoxic Culturing Maintains Activation of Notch and Allows Long-Term Propagation of Human Embryonic Stem Cells without Spontaneous Differentiation. *Cell Proliferation* **2009**, *42*, 63–74, doi:10.1111/j.1365-2184.2008.00571.x.
16. Zachar, V.; Prasad, S.M.; Weli, S.C.; Gabrielsen, A.; Petersen, K.; Petersen, M.B.; Fink, T. The Effect of Human Embryonic Stem Cells (HESCs) Long-Term Normoxic and Hypoxic Cultures on the Maintenance of Pluripotency. *In Vitro Cell.Dev.Biol.-Animal* **2010**, *46*, 276–283, doi:10.1007/s11626-010-9305-3.
17. Harvey, A.J.; Rathjen, J.; Yu, L.J.; Gardner, D.K. Oxygen Modulates Human Embryonic Stem Cell Metabolism in the Absence of Changes in Self-Renewal. *Reprod. Fertil. Dev.* **2016**, *28*, 446, doi:10.1071/RD14013.
18. Lees, J.G.; Rathjen, J.; Sheedy, J.R.; Gardner, D.K.; Harvey, A.J. Distinct Profiles of Human Embryonic Stem Cell Metabolism and Mitochondria Identified by Oxygen. *REPRODUCTION* **2015**, *150*, 367–382, doi:10.1530/REP-14-0633.
19. Rathjen, J.; Yeo, C.; Yap, C.; Tan, B.S.N.; Rathjen, P.D.; Gardner, D.K. Culture Environment Regulates Amino Acid Turnover and Glucose Utilisation in Human ES Cells. *Reprod. Fertil. Dev.* **2014**, *26*, 703, doi:10.1071/RD12276.
20. Dai, Z.; Locasale, J.W. Understanding Metabolism with Flux Analysis: From Theory to Application. *Metabolic Engineering* **2017**, *43*, 94–102, doi:10.1016/j.ymben.2016.09.005.
21. Reid, M.A.; Dai, Z.; Locasale, J.W. The Impact of Cellular Metabolism on Chromatin Dynamics and Epigenetics. *Nat Cell Biol* **2017**, *19*, 1298–1306, doi:10.1038/ncb3629.
22. Wu, J.; Ocampo, A.; Belmonte, J.C.I. Cellular Metabolism and Induced Pluripotency. *Cell* **2016**, *166*, 1371–1385, doi:10.1016/j.cell.2016.08.008.
23. Folmes, C.D.L.; Dzeja, P.P.; Nelson, T.J.; Terzic, A. Metabolic Plasticity in Stem Cell Homeostasis and Differentiation. *Cell Stem Cell* **2012**, *11*, 596–606, doi:10.1016/j.stem.2012.10.002.
24. Lunt, S.Y.; Vander Heiden, M.G. Aerobic Glycolysis: Meeting the Metabolic Requirements of Cell Proliferation. *Annu. Rev. Cell Dev. Biol.* **2011**, *27*, 441–464, doi:10.1146/annurev-cellbio-092910-154237.
25. Tsogtbaatar, E.; Landin, C.; Minter-Dykhouse, K.; Folmes, C.D.L. Energy Metabolism Regulates Stem Cell Pluripotency. *Front. Cell Dev. Biol.* **2020**, *8*, 87, doi:10.3389/fcell.2020.00087.
26. Harvey, A.J.; Rathjen, J.; Gardner, D.K. Metaboloepigenetic Regulation of Pluripotent Stem Cells. *Stem Cells International* **2016**, *2016*, 1–15, doi:10.1155/2016/1816525.
27. Cezar, G.G.; Quam, J.A.; Smith, A.M.; Rosa, G.J.M.; Piekarczyk, M.S.; Brown, J.F.; Gage, F.H.; Muotri, A.R. Identification of Small Molecules from Human Embryonic Stem Cells Using Metabolomics. *Stem Cells and Development* **2007**, *16*, 869–882, doi:10.1089/scd.2007.0022.
28. Gao, Q.; Lee, W.-Y. Urinary Metabolites for Urological Cancer Detection: A Review on the Application of Volatile Organic Compounds for Cancers. *Am J Clin Exp Urol* **2019**, *7*, 232–248.
29. León, Z.; García-Cañaveras, J.C.; Donato, M.T.; Lahoz, A. Mammalian Cell Metabolomics: Experimental Design and Sample Preparation: General. *ELECTROPHORESIS* **2013**, n/a-n/a, doi:10.1002/elps.201200605.
30. Acevedo, C.A.; Sánchez, E.Y.; Reyes, J.G.; Young, M.E. Volatile Organic Compounds Produced by Human Skin Cells. *Biol. Res.* **2007**, *40*, doi:10.4067/S0716-97602007000400009.

31. Zhang, Z.-M.; Cai, J.-J.; Ruan, G.-H.; Li, G.-K. The Study of Fingerprint Characteristics of the Emanations from Human Arm Skin Using the Original Sampling System by SPME-GC/MS. *Journal of Chromatography B* **2005**, *822*, 244–252, doi:10.1016/j.jchromb.2005.06.026.
32. Perez-Ramirez, C.A.; Christofk, H.R. Challenges in Studying Stem Cell Metabolism. *Cell Stem Cell* **2021**, *28*, 409–423, doi:10.1016/j.stem.2021.02.016.
33. Zhang, A.; Sun, H.; Wang, P.; Han, Y.; Wang, X. Modern Analytical Techniques in Metabolomics Analysis. *Analyst* **2012**, *137*, 293–300, doi:10.1039/C1AN15605E.
34. Bischoff, A.-C.; Oertel, P.; Sukul, P.; Rimmbach, C.; David, R.; Schubert, J.; Miekisch, W. Smell of Cells: Volatile Profiling of Stem- and Non-Stem Cell Proliferation. *J. Breath Res.* **2018**, *12*, 026014, doi:10.1088/1752-7163/aaa111.
35. Capuano, R.; Spitalieri, P.; Talarico, R.V.; Domakoski, A.C.; Catini, A.; Paolesse, R.; Martinelli, E.; Novelli, G.; Sangiuolo, F.; Di Natale, C. A Preliminary Analysis of Volatile Metabolites of Human Induced Pluripotent Stem Cells along the in Vitro Differentiation. *Sci Rep* **2017**, *7*, 1621, doi:10.1038/s41598-017-01790-5.
36. Abdal Dayem, A.; Lee, S.; Y. Choi, H.; Cho, S.-G. The Impact of Adhesion Molecules on the In Vitro Culture and Differentiation of Stem Cells. *Biotechnol. J.* **2018**, *13*, 1700575, doi:10.1002/biot.201700575.
37. Smith, D.; Španěl, P. Selected Ion Flow Tube Mass Spectrometry (SIFT-MS) for on-Line Trace Gas Analysis. *Mass Spectrom. Rev.* **2005**, *24*, 661–700, doi:10.1002/mas.20033.
38. Smith, D.; Španěl, P.; Herbig, J.; Beauchamp, J. Mass Spectrometry for Real-Time Quantitative Breath Analysis. *J. Breath Res.* **2014**, *8*, 027101, doi:10.1088/1752-7155/8/2/027101.
39. Smith, D.; Španěl, P. Direct, Rapid Quantitative Analyses of BVOCs Using SIFT-MS and PTR-MS Obviating Sample Collection. *TrAC Trends in Analytical Chemistry* **2011**, *30*, 945–959, doi:10.1016/j.trac.2011.05.001.
40. Španěl, P.; Smith, D. Progress in SIFT-MS: Breath Analysis and Other Applications: PROGRESS IN SIFT-MS. *Mass Spectrom. Rev.* **2011**, *30*, 236–267, doi:10.1002/mas.20303.
41. Aflatoonian, B.; Ruban, L.; Shamsuddin, S.; Baker, D.; Andrews, P.; Moore, H. Generation of Sheffield (Shef) Human Embryonic Stem Cell Lines Using a Microdrop Culture System. *In Vitro Cell.Dev.Biol.-Animal* **2010**, *46*, 236–241, doi:10.1007/s11626-010-9294-2.
42. Cheng, A.; Kapacee, Z.; Peng, J.; Lu, S.; Lucas, R.J.; Hardingham, T.E.; Kimber, S.J. Cartilage Repair Using Human Embryonic Stem Cell-Derived Chondroprogenitors: Human Pluripotent Stem Cells for Cartilage Repair. *STEM CELLS Translational Medicine* **2014**, *3*, 1287–1294, doi:10.5966/sctm.2014-0101.
43. Kumar, D.; Dale, T.P.; Yang, Y.; Forsyth, N.R. Self-Renewal of Human Embryonic Stem Cells on Defined Synthetic Electrospun Nanofibers. *Biomed. Mater.* **2015**, *10*, 065017, doi:10.1088/1748-6041/10/6/065017.
44. Španěl, P.; Smith, D. Selected Ion Flow Tube Mass Spectrometry Analyses of Stable Isotopes in Water: Isotopic Composition of H3O+ and H3O+(H2O)3 Ions in Exchange Reactions with Water Vapor. *J Am Soc Mass Spectrom* **2000**, *11*, 866–875, doi:10.1016/S1044-0305(00)00157-4.
45. Spooner, A.D.; Bessant, C.; Turner, C.; Knobloch, H.; Chambers, M. Evaluation of a Combination of SIFT-MS and Multivariate Data Analysis for the Diagnosis of Mycobacterium Bovis in Wild Badgers. *Analyst* **2009**, *134*, 1922, doi:10.1039/b905627k.
46. Shestivska, V.; Antonowicz, S.S.; Dryahina, K.; Kubišta, J.; Smith, D.; Španěl, P. Direct Detection and Quantification of Malondialdehyde Vapour in Humid Air Using Selected Ion Flow Tube Mass Spectrometry Supported by Gas Chromatography/Mass Spectrometry: SIFT-MS of Malondialdehyde. *Rapid Commun. Mass Spectrom.* **2015**, *29*, 1069–1079, doi:10.1002/rcm.7198.
47. The International Stem Cell Initiative Characterization of Human Embryonic Stem Cell Lines by the International Stem Cell Initiative. *Nat Biotechnol* **2007**, *25*, 803–816, doi:10.1038/nbt1318.

48. Draper, J.S.; Pigott, C.; Thomson, J.A.; Andrews, P.W. Surface Antigens of Human Embryonic Stem Cells: Changes upon Differentiation in Culture*. *J Anatomy* **2002**, *200*, 249–258, doi:10.1046/j.1469-7580.2002.00030.x.
49. Serio, R.N.; Gudas, L.J. Modification of Stem Cell States by Alcohol and Acetaldehyde. *Chemico-Biological Interactions* **2020**, *316*, 108919, doi:10.1016/j.cbi.2019.108919.
50. Seitz, H.K.; Stickel, F. Acetaldehyde as an Underestimated Risk Factor for Cancer Development: Role of Genetics in Ethanol Metabolism. *Genes Nutr* **2010**, *5*, 121–128, doi:10.1007/s12263-009-0154-1.
51. Forsyth, N.R.; Kay, A.; Hampson, K.; Downing, A.; Talbot, R.; McWhir, J. Transcriptome Alterations Due to Physiological Normoxic (2% O_2) Culture of Human Embryonic Stem Cells. *Regenerative Medicine* **2008**, *3*, 817–833, doi:10.2217/17460751.3.6.817.
52. *Metabolic Profiling: Its Role in Biomarker Discovery and Gene Function Analysis*; Harrigan, G.G., Goodacre, R., Eds.; Kluwer Academic: Boston, Mass, 2003; ISBN 978-1-4020-7370-0.
53. Calenic, B.; Amann, A. Detection of Volatile Malodorous Compounds in Breath: Current Analytical Techniques and Implications in Human Disease. *Bioanalysis* **2014**, *6*, 357–376, doi:10.4155/bio.13.306.
54. Wardencki, W.; Chmiel, T.; Dymerski, T. Gas Chromatography-Olfactometry (GC-O), Electronic Noses (e-Noses) and Electronic Tongues (e-Tongues) for in Vivo Food Flavour Measurement. In *Instrumental Assessment of Food Sensory Quality*; Elsevier, 2013; pp. 195–229 ISBN 978-0-85709-439-1.
55. Harper, W.J. The Strengths and Weaknesses of the Electronic Nose. In *Headspace Analysis of Foods and Flavors*; Rouseff, R.L., Cadwallader, K.R., Eds.; Advances in Experimental Medicine and Biology; Springer US: Boston, MA, 2001; Vol. 488, pp. 59–71 ISBN 978-1-4613-5460-4.
56. Lees, J.G.; Cliff, T.S.; Gammilonghi, A.; Ryall, J.G.; Dalton, S.; Gardner, D.K.; Harvey, A.J. Oxygen Regulates Human Pluripotent Stem Cell Metabolic Flux. *Stem Cells International* **2019**, *2019*, 1–17, doi:10.1155/2019/8195614.
57. Cahan, P.; Daley, G.Q. Origins and Implications of Pluripotent Stem Cell Variability and Heterogeneity. *Nat Rev Mol Cell Biol* **2013**, *14*, 357–368, doi:10.1038/nrm3584.
58. Chin, M.H.; Mason, M.J.; Xie, W.; Volinia, S.; Singer, M.; Peterson, C.; Ambartsumyan, G.; Aimiuwu, O.; Richter, L.; Zhang, J.; et al. Induced Pluripotent Stem Cells and Embryonic Stem Cells Are Distinguished by Gene Expression Signatures. *Cell Stem Cell* **2009**, *5*, 111–123, doi:10.1016/j.stem.2009.06.008.
59. Narsinh, K.H.; Plews, J.; Wu, J.C. Comparison of Human Induced Pluripotent and Embryonic Stem Cells: Fraternal or Identical Twins? *Molecular Therapy* **2011**, *19*, 635–638, doi:10.1038/mt.2011.41.
60. Ortmann, D.; Vallier, L. Variability of Human Pluripotent Stem Cell Lines. *Current Opinion in Genetics & Development* **2017**, *46*, 179–185, doi:10.1016/j.gde.2017.07.004.
61. Bock, C.; Kiskinis, E.; Verstappen, G.; Gu, H.; Boulting, G.; Smith, Z.D.; Ziller, M.; Croft, G.F.; Amoroso, M.W.; Oakley, D.H.; et al. Reference Maps of Human ES and IPS Cell Variation Enable High-Throughput Characterization of Pluripotent Cell Lines. *Cell* **2011**, *144*, 439–452, doi:10.1016/j.cell.2010.12.032.
62. Kondoh, H.; Lleonart, M.E.; Nakashima, Y.; Yokode, M.; Tanaka, M.; Bernard, D.; Gil, J.; Beach, D. A High Glycolytic Flux Supports the Proliferative Potential of Murine Embryonic Stem Cells. *Antioxidants & Redox Signaling* **2007**, *9*, 293–299, doi:10.1089/ars.2006.1467.
63. Varum, S.; Rodrigues, A.S.; Moura, M.B.; Momcilovic, O.; Easley, C.A.; Ramalho-Santos, J.; Van Houten, B.; Schatten, G. Energy Metabolism in Human Pluripotent Stem Cells and Their Differentiated Counterparts. *PLoS ONE* **2011**, *6*, e20914, doi:10.1371/journal.pone.0020914.
64. Zhang, J.; Khvorostov, I.; Hong, J.S.; Oktay, Y.; Vergnes, L.; Nuebel, E.; Wahjudi, P.N.; Setoguchi, K.; Wang, G.; Do, A.; et al. UCP2 Regulates Energy Metabolism and Differentiation Potential of Human Pluripotent Stem Cells: UCP2 Regulates HPSC Metabolism and Differentiation. *The EMBO Journal* **2011**, *30*, 4860–4873, doi:10.1038/emboj.2011.401.

65. Zhou, W.; Choi, M.; Margineantu, D.; Margaretha, L.; Hesson, J.; Cavanaugh, C.; Blau, C.A.; Horwitz, M.S.; Hockenbery, D.; Ware, C.; et al. HIF1α Induced Switch from Bivalent to Exclusively Glycolytic Metabolism during ESC-to-EpiSC/HESC Transition: Metabolic Switch in ESC-to-EpiSC/HESC Transition. *The EMBO Journal* **2012**, *31*, 2103–2116, doi:10.1038/emboj.2012.71.
66. Fynes, K.; Tostoes, R.; Ruban, L.; Weil, B.; Mason, C.; Veraitch, F.S. The Differential Effects of 2% Oxygen Preconditioning on the Subsequent Differentiation of Mouse and Human Pluripotent Stem Cells. *Stem Cells and Development* **2014**, *23*, 1910–1922, doi:10.1089/scd.2013.0504.
67. Xie, Y.; Zhang, J.; Lin, Y.; Gaeta, X.; Meng, X.; Wisidagama, D.R.R.; Cinkornpumin, J.; Koehler, C.M.; Malone, C.S.; Teitell, M.A.; et al. Defining the Role of Oxygen Tension in Human Neural Progenitor Fate. *Stem Cell Reports* **2014**, *3*, 743–757, doi:10.1016/j.stemcr.2014.09.021.
68. Podkalicka, P.; Stępniewski, J.; Mucha, O.; Kachamakova-Trojanowska, N.; Dulak, J.; Łoboda, A. Hypoxia as a Driving Force of Pluripotent Stem Cell Reprogramming and Differentiation to Endothelial Cells. *Biomolecules* **2020**, *10*, 1614, doi:10.3390/biom10121614.
69. Koay, E.J.; Athanasiou, K.A. Hypoxic Chondrogenic Differentiation of Human Embryonic Stem Cells Enhances Cartilage Protein Synthesis and Biomechanical Functionality. *Osteoarthritis and Cartilage* **2008**, *16*, 1450–1456, doi:10.1016/j.joca.2008.04.007.
70. Prado-Lopez, S.; Conesa, A.; Armiñán, A.; Martínez-Losa, M.; Escobedo-Lucea, C.; Gandia, C.; Tarazona, S.; Melguizo, D.; Blesa, D.; Montaner, D.; et al. Hypoxia Promotes Efficient Differentiation of Human Embryonic Stem Cells to Functional Endothelium. *STEM CELLS* **2010**, *28*, 407–418, doi:10.1002/stem.295.
71. Cui, P.; Zhang, P.; Zhang, Y.; Sun, L.; Cui, G.; Guo, X.; Wang, H.; Zhang, X.; Shi, Y.; Yu, Z. HIF-1α/Actl6a/H3K9ac Axis Is Critical for Pluripotency and Lineage Differentiation of Human Induced Pluripotent Stem Cells. *FASEB j.* **2020**, *34*, 5740–5753, doi:10.1096/fj.201902829RR.
72. Bae, D.; Mondragon-Teran, P.; Hernandez, D.; Ruban, L.; Mason, C.; Bhattacharya, S.S.; Veraitch, F.S. Hypoxia Enhances the Generation of Retinal Progenitor Cells from Human Induced Pluripotent and Embryonic Stem Cells. *Stem Cells and Development* **2012**, *21*, 1344–1355, doi:10.1089/scd.2011.0225.
73. Hakim, F.; Kaitsuka, T.; Raeed, J.Mohd.; Wei, F.-Y.; Shiraki, N.; Akagi, T.; Yokota, T.; Kume, S.; Tomizawa, K. High Oxygen Condition Facilitates the Differentiation of Mouse and Human Pluripotent Stem Cells into Pancreatic Progenitors and Insulin-Producing Cells. *Journal of Biological Chemistry* **2014**, *289*, 9623–9638, doi:10.1074/jbc.M113.524363.
74. Worley, B.; Powers, R. PCA as a Practical Indicator of OPLS-DA Model Reliability. *Curr Metabolomics* **2016**, *4*, 97–103, doi:10.2174/2213235X04666160613122429.
75. Španěl, P.; Smith, D. Quantification of Volatile Metabolites in Exhaled Breath by Selected Ion Flow Tube Mass Spectrometry, SIFT-MS. *Clinical Mass Spectrometry* **2020**, *16*, 18–24, doi:10.1016/j.clinms.2020.02.001.
76. Osafune, K.; Caron, L.; Borowiak, M.; Martinez, R.J.; Fitz-Gerald, C.S.; Sato, Y.; Cowan, C.A.; Chien, K.R.; Melton, D.A. Marked Differences in Differentiation Propensity among Human Embryonic Stem Cell Lines. *Nat Biotechnol* **2008**, *26*, 313–315, doi:10.1038/nbt1383.
77. Boulting, G.L.; Kiskinis, E.; Croft, G.F.; Amoroso, M.W.; Oakley, D.H.; Wainger, B.J.; Williams, D.J.; Kahler, D.J.; Yamaki, M.; Davidow, L.; et al. A Functionally Characterized Test Set of Human Induced Pluripotent Stem Cells. *Nat Biotechnol* **2011**, *29*, 279–286, doi:10.1038/nbt.1783.
78. Capuano, R.; Spitalieri, P.; Talarico, R.V.; Catini, A.; Domakoski, A.C.; Martinelli, E.; Scioli, M.G.; Orlandi, A.; Cicconi, R.; Paolesse, R.; et al. Volatile Compounds Emission from Teratogenic Human Pluripotent Stem Cells Observed during Their Differentiation in Vivo. *Sci Rep* **2018**, *8*, 11056, doi:10.1038/s41598-018-29212-0.
79. Sulé-Suso, J.; Forsyth, N.R.; Untereiner, V.; Sockalingum, G.D. Vibrational Spectroscopy in Stem Cell Characterisation: Is There a Niche? *Trends in Biotechnology* **2014**, *32*, 254–262, doi:10.1016/j.tibtech.2014.03.002.

80. Parrotta, E.; De Angelis, M.T.; Scalise, S.; Candeloro, P.; Santamaria, G.; Paonessa, M.; Coluccio, M.L.; Perozziello, G.; De Vitis, S.; Sgura, A.; et al. Two Sides of the Same Coin? Unraveling Subtle Differences between Human Embryonic and Induced Pluripotent Stem Cells by Raman Spectroscopy. *Stem Cell Res Ther* **2017**, *8*, 271, doi:10.1186/s13287-017-0720-1.
81. Chan, J.W.; Lieu, D.K.; Huser, T.; Li, R.A. Label-Free Separation of Human Embryonic Stem Cells and Their Cardiac Derivatives Using Raman Spectroscopy. *Anal. Chem.* **2009**, *81*, 1324–1331, doi:10.1021/ac801665m.
82. Schulze, H.G.; Konorov, S.O.; Caron, N.J.; Piret, J.M.; Blades, M.W.; Turner, R.F.B. Assessing Differentiation Status of Human Embryonic Stem Cells Noninvasively Using Raman Microspectroscopy. *Anal. Chem.* **2010**, *82*, 5020–5027, doi:10.1021/ac902697q.
83. Konorov, S.O.; Schulze, H.G.; Piret, J.M.; Aparicio, S.A.; Turner, R.F.B.; Blades, M.W. Raman Microscopy-Based Cytochemical Investigations of Potential Niche-Forming Inhomogeneities Present in Human Embryonic Stem Cell Colonies. *Appl Spectrosc* **2011**, *65*, 1009–1016, doi:10.1366/11-06312.
84. Tan, Y.; Konorov, S.O.; Schulze, H.G.; Piret, J.M.; Blades, M.W.; Turner, R.F.B. Comparative Study Using Raman Microspectroscopy Reveals Spectral Signatures of Human Induced Pluripotent Cells More Closely Resemble Those from Human Embryonic Stem Cells than Those from Differentiated Cells. *Analyst* **2012**, *137*, 4509, doi:10.1039/c2an35507h.
85. Heraud, P.; Ng, E.S.; Caine, S.; Yu, Q.C.; Hirst, C.; Mayberry, R.; Bruce, A.; Wood, B.R.; McNaughton, D.; Stanley, E.G.; et al. Fourier Transform Infrared Microspectroscopy Identifies Early Lineage Commitment in Differentiating Human Embryonic Stem Cells. *Stem Cell Research* **2010**, *4*, 140–147, doi:10.1016/j.scr.2009.11.002.
86. Smith, D.; Wang, T.; Sulé-Suso, J.; Španěl, P.; Haj, A.E. Quantification of Acetaldehyde Released by Lung Cancer Cells *in Vitro* Using Selected Ion Flow Tube Mass Spectrometry: Acetaldehyde from Lung Cancer Cells. *Rapid Commun. Mass Spectrom.* **2003**, *17*, 845–850, doi:10.1002/rcm.984.
87. Shin, H.-W.; Umber, B.J.; Meinardi, S.; Leu, S.-Y.; Zaldivar, F.; Blake, D.R.; Cooper, D.M. Acetaldehyde and Hexanaldehyde from Cultured White Cells. *J Transl Med* **2009**, *7*, 31, doi:10.1186/1479-5876-7-31.
88. Rutter, A.V.; Chippendale, T.W.E.; Yang, Y.; Španěl, P.; Smith, D.; Sulé-Suso, J. Quantification by SIFT-MS of Acetaldehyde Released by Lung Cells in a 3D Model. *Analyst* **2013**, *138*, 91–95, doi:10.1039/C2AN36185J.
89. Sulé-Suso, J.; Pysanenko, A.; Španěl, P.; Smith, D. Quantification of Acetaldehyde and Carbon Dioxide in the Headspace of Malignant and Non-Malignant Lung Cells in Vitro by SIFT-MS. *Analyst* **2009**, *134*, 2419, doi:10.1039/b916158a.
90. Zhang, J.; Nuebel, E.; Wisidagama, D.R.R.; Setoguchi, K.; Hong, J.S.; Van Horn, C.M.; Imam, S.S.; Vergnes, L.; Malone, C.S.; Koehler, C.M.; et al. Measuring Energy Metabolism in Cultured Cells, Including Human Pluripotent Stem Cells and Differentiated Cells. *Nat Protoc* **2012**, *7*, 1068–1085, doi:10.1038/nprot.2012.048.
91. Lees, J.G.; Gardner, D.K.; Harvey, A.J. Pluripotent Stem Cell Metabolism and Mitochondria: Beyond ATP. *Stem Cells International* **2017**, *2017*, 1–17, doi:10.1155/2017/2874283.
92. Simsek, T.; Kocabas, F.; Zheng, J.; Deberardinis, R.J.; Mahmoud, A.I.; Olson, E.N.; Schneider, J.W.; Zhang, C.C.; Sadek, H.A. The Distinct Metabolic Profile of Hematopoietic Stem Cells Reflects Their Location in a Hypoxic Niche. *Cell Stem Cell* **2010**, *7*, 380–390, doi:10.1016/j.stem.2010.07.011.
93. Takubo, K.; Goda, N.; Yamada, W.; Iriuchishima, H.; Ikeda, E.; Kubota, Y.; Shima, H.; Johnson, R.S.; Hirao, A.; Suematsu, M.; et al. Regulation of the HIF-1α Level Is Essential for Hematopoietic Stem Cells. *Cell Stem Cell* **2010**, *7*, 391–402, doi:10.1016/j.stem.2010.06.020.
94. Mucaj, V.; Shay, J.E.S.; Simon, M.C. Effects of Hypoxia and HIFs on Cancer Metabolism. *Int J Hematol* **2012**, *95*, 464–470, doi:10.1007/s12185-012-1070-5.
95. Masson, N.; Ratcliffe, P.J. Hypoxia Signaling Pathways in Cancer Metabolism: The Importance of Co-Selecting Interconnected Physiological Pathways. *Cancer Metab* **2014**, *2*, 3, doi:10.1186/2049-3002-2-3.

96. Guan, X.-L.; Wu, P.-F.; Wang, S.; Zhang, J.-J.; Shen, Z.-C.; Luo, H.; Chen, H.; Long, L.-H.; Chen, J.-G.; Wang, F. Dimethyl Sulfide Protects against Oxidative Stress and Extends Lifespan via a Methionine Sulfoxide Reductase A-Dependent Catalytic Mechanism. *Aging Cell* **2017**, *16*, 226–236, doi:10.1111/acel.12546.
97. TÃ¶pfer, N.; Kleessen, S.; Nikoloski, Z. Integration of Metabolomics Data into Metabolic Networks. *Front. Plant Sci.* **2015**, *6*, doi:10.3389/fpls.2015.00049.
98. Mo, M.L.; Palsson, B.Ø.; Herrgård, M.J. Connecting Extracellular Metabolomic Measurements to Intracellular Flux States in Yeast. *BMC Syst Biol* **2009**, *3*, 37, doi:10.1186/1752-0509-3-37.